



MÉRNÖKI ÉS INFORMATIKAI MEGOLDÁSOK

ENGINEERING AND IT SOLUTIONS

EÖTVÖS LORÁND UNIVERSITY
FACULTY OF INFORMATICS
SAVARIA INSTITUTE OF TECHNOLOGY



II. 2020.

MÉRNÖKI ÉS INFORMATIKAI MEGOLDÁSOK
ENGINEERING AND IT SOLUTIONS

II. 2020.

IMPRESS

Editor-in-Chief

Dr. Ferenc Safranyik

Editors

Dr. Mátyás Andó

Prof. Dr. Jurij Sidor

Editorial board

Dr. Árpád Bak	Prof. Dr. Gábor Kalácska
Dr. István Barányi	Prof. Dr. István Keppler
Dr. Gergely Bencsik	Dr. Róbert Zsolt Keresztes
Dr. Imre Czupy	Prof. Dr. László Kollár
Prof. Dr. András Eleőd	Dr. Zoltán Pödör
Dr. Gábor Farkas	Dr. Zoltán Szakál
Dr. Gusztáv Fekete	Dr. Béla János Szekeres
Dr. Dániel Fenyvesi	Dr. Attila Varga
Dr. László Gál	Dr. László Zsidai
Prof. Dr. Béla Horváth	

Publisher

Eötvös Loránd University, Faculty of Informatics
Savaria Institute of Technology
Prof. Dr. László Kollár, head of institute

Cover design

Dr. Ferenc Safranyik

HU ISSN 2677-1691

© ELTE, Faculty of Informatics, Savaria Institute of Technology, 2020.

HU-9700, Szombathely, Károlyi Gáspár tér. 4.

Contact: sf@inf.elte.hu, [URL](#)

TABLE OF CONTENTS

Foreword	4
Gábor Farkas, Zsombor Kiss, Dániel Papatyi, Krisztina Schäffer, Prime Hunting	5
János Hegedűs-Kuti, Mátyás Andó, Performance of Cell Phone Controlled Model Vehicle	14
Boldizsár Könczöl, László Gál, Analysing fuzzy logic-based line following model car	21
Luis Rubio, Asier Ibeas, László E. Kollár, On the sliding mode control for precision machining	32
László Karker, Mátyás Andó, Jegan Mohan Sudhan Raj, Product configuration system development for CAD/CAM software	42

FOREWORD

The first issue of “Engineering and IT solutions”, published in English, integrates both fundamental and applied knowledge from the area of applied mathematics, system automatization, and computer-aided design. The aim of this hybrid issue is to assimilate various fields related to a vast variety of computational and engineering branches. Journal of “Engineering and IT solutions” creates a solid platform for young researches and experienced scientists for publishing their high-quality contributions in the mentioned fields. The contributed manuscripts perfectly meet the scope of the journal as well as respond to the current technological and IT challenges.

The ongoing automation, related to the so-called 4th industrial revolution, employs recent technologies, which are able to communicate with one another via monitoring IT-based platforms. Digital transformation of production technologies accounts for revolutionary ways of manufacturing, and apart from this, the cyber-physical systems enable in-situ process optimization. In view of the above, integration of diverse fields into interdisciplinary one is of key importance, especially when it comes to engineering and IT technologies, since all modern products have smart features, resulting from the development in both areas.

The publications of this issue deal with a wide spectrum of problems starting with the mathematical abstraction of the building blocks of our universe through the control of machining and model vehicle as well as analysis of fuzzy logic-based trajectories of model cars. All these topics are incorporated in the education programs of mechanical and software engineering BSc, MSc, and doctoral school programs of ELTE University and contribute to the development of new generation technologies.



October, 2020, Szombathely

Prof. Dr. Jurij Sidor
editor

PRIME HUNTING

Gábor Farkas^{a*}, Zsombor Kiss^b, Dániel Papatyi^b, Krisztina Schäffer^b

^a ELTE, Faculty of Informatics, Department of Computer Algebra, associate professor

^b ELTE, Computer Scientist BSc, II. year

ABSTRACT

“Prime hunting” can be considered as a research area of computational number theory. Its goal is to find special combinations of integers and prove their primality. Four research groups, established by A. Járαι between 1992 and 2014, published numerous world class scientific results. In this period, due to Járαι’s arithmetic routines fastest in the world, they reached the world record 19 times, namely found the largest known twin primes 9 times, Sophie Germain primes 7 times, a prime of the form $n^4 + 1$, a number which is simultaneously twin and Sophie Germain prime and the three largest known primes forming a Cunningham chain of length 3 of the first kind. When A. Járαι retired, the investigations of this area were suspended. In the beginning of 2020 the research was reopened by G. Farkas at the newly-founded campus (Szombathely) of ELTE. The first signal success came in the end of May 2020. They proved the primality of the numbers which form the largest known Cunningham chains of length 2 of the 2nd kind. In this paper we report on a newly started prime hunting project with the aim of increasing our students’ research activity.

Keywords: *computational number theory, prime tests, curious prime combinations, prime records*

1. Introduction

A well-organized collection of large prime numbers was started in 1984 when the name “Titanic Prime” was given to the primes with more than 1000 decimal digits by S. Yates [1]. We can say that a contest started for primes categorized by their “archivable” form. The exact definition of archivable form can be found on the site [2] which is supervised by C. K. Caldwell since 1996. For example, twin, Sophie Germain and Mersenne are well-known archivable forms. On Caldwell’s site a top list can be seen for each form which contains the largest known primes in that category.

Reading about a world record prime, a question always arises as to why people want to find these numbers. In our point of view there are many reasons, for example knowing the newest scientific results and methods, designing and developing fast and effective programs, testing the hardware and continuing a beautiful tradition. From ≈ 300 BC to 2020 numerous famous mathematicians became “large prime collectors”, for example Euclid, Descartes, Fermat, Mersenne, Leibniz, Euler, Lucas, Catalan, Cunningham, Pepin, Putnam, Lehmer and Járαι.

2. Prime tests

A prime hunting process can be divided into two main parts, namely the sieving and primality checking. In this chapter we focus our attention to the theoretical background of prime tests.

© ELTE, Faculty of Informatics, Savaria Institute of Technology, 2020

*Corresponding author: Gábor Farkas, farkasg@inf.elte.hu

<https://doi.org/10.37775/EIS.2020.2.1>

2.1. Conclusive Prime Tests

Deciding whether a given number n is prime or not, is a problem that has interested mathematicians for ages. The oldest algorithm is more than 2500 years old, aptly called trial division, it simply checks if any number smaller than n divides it or not. The algorithm can be improved by noticing that one only needs to check for prime divisors less or equal than \sqrt{n} , however this is still extremely slow. Trial division, combined with other more efficient methods, is still used to this day for testing whether a number has small prime factors [3].

There are much faster modern algorithms – such as the AKS primality test – that is proven to run in polynomial time and ECPP, which can be proven to also run in polynomial time contingent on some conjectures [3]. Significantly better running times can be achieved with simpler algorithms if we only consider numbers of special forms. Two such tests are the *Reisel test* and the *Proth test*.

Proth test

The Proth test is a primality test for numbers of the form $N = k \cdot 2^n + 1$, where k is odd and $2^n > k$. These numbers are known as Proth numbers. The algorithm is based on the following theorem published in 1878 [4]:

Theorem 2.1 (*Proth's theorem*) *Let N be as described above, if there exists an integer a such that*

$$a^{(N-1)/2} \equiv -1 \pmod{N},$$

then N is prime.

There is no efficient strategy to find such an a , therefore the test's running time varies randomly.

Riesel test

Let $N = h \cdot 2^n - 1$, such that $2 \leq n \in \mathbb{N}$, $2^n > h \in \mathbb{Z}^+$ is odd, $D > 1$ a square-free positive integer, $a, b \in \mathbb{Z}$, $r = |a^2 - b^2 D|$, $\alpha = (a + b\sqrt{D})^2/r \in I_D$ the ring of algebraic integers (quadratic integers) of the quadratic field of $\mathbb{Q}(\sqrt{D})$, furthermore suppose that:

$$\left(\frac{D}{N}\right) = -1, \quad (1)$$

$$\left(\frac{r}{N}\right) (a^2 - b^2 D)/r = -1, \quad (2)$$

where $\left(\frac{D}{N}\right)$ is the Jacobi symbol, which is an extension of the Legendre symbol. Let m be an integer, p a prime, then the Legendre symbol is defined as:

$$\left(\frac{m}{p}\right) = \begin{cases} 0 & \text{if } p \mid m, \\ 1 & \text{if } p \nmid m \text{ and } x^2 \equiv m \pmod{p} \text{ has a solution,} \\ -1 & \text{if } p \nmid m \text{ and } x^2 \equiv m \pmod{p} \text{ has no solution.} \end{cases}$$

The Jacobi symbol is the unique extension of the Legendre symbol to all positive odd integers $n = b \cdot c$ with the multiplicative property:

$$\left(\frac{m}{n}\right) = \left(\frac{m}{b}\right) \cdot \left(\frac{m}{c}\right).$$

Now, we can formulate Riesel's famous assertion:

Theorem 2.2 *Suppose the above conditions hold, then N is prime if and only if*

$$u_{n-2} = \alpha^{h2^{n-2}} + \alpha^{-h2^{n-2}} \equiv 0 \pmod{N},$$

where $u_0 = \alpha^h + \alpha^{-h}$ and $u_i = u_{i-1}^2 - 2$.

H. Riesel published the proof in [5]. We show an example where we set $D = 13$, $a = 3$, and $b = 1$ as hyperparameters. Using a method described in [6] we can always find values h for which Eq. (1) holds. Eq. (2) always holds because $r = 4$, so

$$\left(\frac{r}{N}\right) = \left(\frac{2^2}{N}\right) = \left(\frac{2}{N}\right)^2$$

which can only equal 1 since N is odd.

We represented quadratic integers in the form

$$x + y \cdot \frac{(1 + \sqrt{13})}{2}$$

with x and y being integers. First we computed

$$\alpha^h = x + y \cdot \frac{(1 + \sqrt{13})}{2}$$

with a simple repeated-squaring algorithm implemented by us for quadratic integers, analogous to the one for rational integers in [7]. After that we stored

$$\alpha^h + \alpha^{-h} = 2 \cdot x + y$$

and used the identity $c^2 + c^{-2} = (c + c^{-1})^2 - 2$ for $c = \alpha^{h2^i}$ to compute

$$\alpha^{h2^{n-2}} + \alpha^{-h2^{n-2}}$$

working with rational integers instead of quadratic integers.

Since we only use this test to verify the primality of just a few numbers, extreme efficiency is not necessary. For example, in the case $n = 36\,627$ and $h = 778\,965\,587\,811$ our implementation was able to verify the number's primality in 7.72784 seconds.

2.2. Probabilistic primality tests

Probabilistic tests, as opposed to deterministic ones, do not always correctly answer whether a given number is prime or not, but they are often the preferred choice in practice, as they are significantly faster and there is only a small chance that they are mistaken (around one in a billion).

One of the simplest probabilistic tests is the *Fermat test*, in which we simply compute $a^{n-1} \pmod{n}$, for an arbitrary base a relatively prime to n . The result is 1 if n is prime, according to Fermat's Little Theorem, and is different from 1 with good chance if n is composite.

The *Fermat test* can be improved if we consider only odd candidates $n > 8$ and write them as

$$n = 1 + q \cdot 2^k,$$

where q is odd. If n is prime, once again applying Fermat's Little Theorem we get

$$a^{q \cdot 2^k} \equiv 1 \pmod{n}.$$

Upon further consideration, we can notice that if n is prime,

$$x^2 \equiv 1 \pmod{n}$$

if and only if

$$x^2 - 1 = (x + 1)(x - 1) \equiv 0 \pmod{n}.$$

Thus, $x \equiv 1$ or $x \equiv -1$, e.g. $a^{q \cdot 2^k} \equiv 1$ if and only if $a^q \equiv 1$ or $a^{q \cdot 2^j} \equiv -1$ for some $0 \leq j \leq k - 1$, which can easily be checked during the computation of $a^{q \cdot 2^{k-1}} \pmod{n}$. This method is known as the *Miller–Rabin test* [3].

We compared the execution times of these algorithms for $a = 2$, and numbers of the form $h \cdot 2^m - 1$, because only these were considered in our prime hunting project. As expected, there was no noticeable difference, in fact since $h \cdot 2^m - 1 = 2 \cdot (h \cdot 2^{m-1} - 1) + 1$ only one extra comparison had to be made in the *Miller–Rabin test*.

The *Miller–Rabin test* can be converted into a deterministic test by testing for several bases, and applying a bound on the maximum number of bases that give false positives (these bases are known as liars). One such bound is $n/4$, which can be obtained by elementary considerations, but this results in a rather slow algorithm. There is a significantly better bound, but unfortunately it relies on the Generalised Riemann Hypothesis being true, so the *Miller–Rabin test* is not used as a deterministic test.

Theorem 2.3 *Let $n > 8$ be a non-prime power composite number, if the Generalised Riemann Hypothesis is true, then there exists a base*

$$a < 2(\ln(n))^2$$

with which the Miller–Rabin-test discovers that n is composite.

Algorithm 1 The pseudocode of the Miller–Rabin primality test

<pre> 1: procedure MILLERRABIN(n) 2: $a \leftarrow 2$ 3: $k \leftarrow \log_2(n - 1)/2$ 4: $j \leftarrow k$ 5: $b \leftarrow a^q \pmod{n}$ 6: if ((($j = k$) and ($b = 1$)) or ($b = n - 1$)) then 7: return probably prime 8: end if 9: if (($j < k$) and ($b = 1$)) then 10: return composite 11: end if 12: $j \leftarrow j - 1$ 13: if ($j > 0$) then 14: $b \leftarrow b^2 \pmod{n}$ 15: goto 6 16: end if 17: return composite 18: end procedure </pre>	<p>▷ Miller–Rabin primality test</p>
---------------------------------------------------------------------------------------------------------------------------------------------------------------------------------------------------------------------------------------------------------------------------------------------------------------------------------------------------------------------------------------------------------------------------------------------------------------------------------------------------------------------------------------------------------------------------------------------------------------------------------------------------------------------------------------------------------------------------------------------------------------	--------------------------------------

For the above mentioned prime tests Z. Kiss and D. Papatyi gave their own implementation in our project. We plan to use these routines in a prime hunting project in the near future, therefore we are working on further improving the efficiency of these programs. The pseudocode of the *Miller–Rabin test* can be seen in [Algorithm 1](#).

3. Prime hunting

Since our prospective purpose is to reach such results as Járαι et al. published in [8-21], apart from primality tests, we also have to implement some efficient sieving programs. In the following part of this paper the work described in [9] is called *Cc22 – project*.

We focus on the following archivable forms: twin primes, Sophie Germain primes and Cunningham chains.

Definition 3.1 *Let p be a prime. If*

- $p + 2$ is also a prime then p and $p + 2$ are *twin primes*,
- $2p + 1$ is also a prime then p is a *Sophie Germain prime*,
- $2p + 1$ and $4p + 3$ are primes then p is a *double Sophie Germain or safe prime*,
- if we have a sequence of primes

$$\{p, 2p + d, 4p + 3d, 8p + 7d, \dots, 2^{k-1}p + (2^{k-1} - 1)d\},$$

where $k \geq 2$, we speak about a **Cunningham chain of length k of the first kind** (notation: *Cck1*) if $d = 1$ and a **Cunningham chain of length k of the second kind** (notation: *Cck2*) if $d = -1$.

Before programming we need to calculate the value of some important hyperparameters. First of all, we choose a set $H = \{1, 2, \dots, 2^R - 1\}$. To find the value of R the Bateman–Horn conjecture [22] is used. The exact computations of the hyperparameters were published in [23] and [24]. Afterwards we generate sequences of large numbers by substituting the elements of H into *generator polynomials*. These sequences include the prime numbers searched for.

3.1. Generator polynomials

A generator polynomial can be given in the form:

$$f_i(x) = (h_0 + c \cdot x) \cdot 2^{e+i} + j, \quad (3)$$

where j is equal 1 or -1 and $i \in \{0, 1, \dots, l\}$. The description of the integers e , h_0 and c can be seen later in this subsection. The numbers generated by a generator polynomial are called *candidates*. Consider the following deductions: if we set $j = 1$ then for the polynomials

$$f_i(x) = (h_0 + c \cdot x) \cdot 2^{e+i} + 1,$$

where $i = 0, 1$, the equation $f_1 = 2f_0 - 1$ is valid because

$$(h_0 + c \cdot x) \cdot 2^{e+1} + 1 = 2 \cdot ((h_0 + c \cdot x) \cdot 2^e + 1) - 1.$$

Thus, if for an arbitrary $x \in H$, $f_0(x)$ and $f_1(x)$ are simultaneously prime then they form a *Cc22*.

We can observe easily that the polynomials Eq. (3) can generate a *Cck2* for an arbitrary k if $i = 0, 1, \dots, k$ and $f_0(x), f_1(x), \dots, f_k(x)$ are simultaneously primes for some $x \in H$. Furthermore, we can generate sequences for *Cck1* too if we use the value $j = -1$.

Algorithm 2 The pseudocode of the sieving method

```

1: procedure SIEVE( $R, p_S, e, h_0, c$ ) ▷ Sieve
2:    $B[0] \leftarrow 1, B[1] \leftarrow 1, \dots, B[|H| - 1] \leftarrow 1$ 
3:   Produce "small primes"  $P_S$ : primes up to  $p_S$  with sieve of Eratosthenes
4:    $p \leftarrow$  the smallest prime in  $P_S$ 
5:   while  $p \leq p_S$  do
6:     for  $i = 1$  to  $k$  do
7:       Let  $h$  be the solution of the congruence  $f_i(x) \equiv 0 \pmod{p}$ 
8:        $B[h] \leftarrow 0, B[h + p] \leftarrow 0, \dots, B[h + q \cdot p] \leftarrow 0$ , where  $(h + q \cdot p) < |H|, q \in \mathbb{N}$ 
9:     end for
10:     $p \leftarrow \text{nextprime}(p)$ 
11:  end while
12:   $A \leftarrow$  {the indexes of elements 1 in  $B$ }
13:  Do in parallel
14:    Compute thread 1
15:    Compute thread 2
16:     $\vdots$ 
17:    Compute thread  $n$ 
18:  EndDo
19:   $\overline{A} \leftarrow \bigcap_{j=1}^n A_j$ 
20:  return  $\overline{A}$ 
21: end procedure

```

If we hunt for twin primes the appropriate generator polynomials are

$$f_i(x) = (h_0 + c \cdot x) \cdot 2^e + (-1)^{i+1},$$

where $i = 0, 1$.

Consider now the other hyperparameters. The constant h_0 guarantees that the generated numbers satisfy the Lucasian criteria for the Riesel primality test shown in the previous section. The constant e is called the exponent and it sets the magnitude of the generated numbers. The constant c is the product of the first k prime numbers:

$$c = p_1 \cdot p_2 \cdot \dots \cdot p_k,$$

where $k \in \mathbb{N}^+$ and p_i is the i -th prime. If we correctly set the values of the parameters e , h_0 and c then the numbers generated by polynomials of the form Eq. (3) are sufficiently large, satisfy the conditions of the Riesel test and do not have prime factors $p|c$.

If the goal is to generate numbers of the form $k \cdot 2^n + 1$ then $h_0 = 0$ can be chosen. For example, Farkas et al in *Cc22 – project* set the parameters in the following way: $h_0 = 0$, $c = 30030$ and $e = 256000$. Thus, the generated numbers had no prime factors less than 17 and had at least 77 069 decimal digits.

3.2. Sieving

The primality tests are highly time-consuming therefore the number of candidates must be reduced. In order to explain our method, we introduce some new concepts. Consider the set $P_S = \{p_{k+1}, p_{k+2}, \dots, p_S\}$ which contains all prime numbers between p_{k+1} , the smallest prime which

Algorithm 3 The pseudocode of thread i

```

1: procedure THREAD  $i(A, p_a, p_b)$   $\triangleright p_a, p_b$  are primes and  $p_S < p_a < p_b < p_S^2$ 
2:    $A_i \leftarrow A$ 
3:   Produce "small primes"  $P_S$ : primes up to  $p_S$  with sieve of Eratosthenes
4:   while  $\exists p \in P_L$  where  $p$  has not yet been used as a sieving prime do
5:     while  $p < p_b$  do
6:       Produce the primes from  $p_a$  to  $p_b \rightarrow PST$  with sieve of Eratosthenes
7:        $p \leftarrow$  the smallest element of  $PST$ 
8:       for  $j = 1$  to  $k$  do
9:         Let  $h$  be the solution of the congruence  $f_j(x) \equiv 0 \pmod{p}$ 
10:         $A_i \leftarrow A_i \setminus \{h, h + 2p, \dots, h + q \cdot p < |H|\}$ 
11:       end for
12:        $p \leftarrow \text{nextprime}(p)$ 
13:     end while
14:     Update  $p_a$  and  $p_b$ 
15:   end while
16:   return  $A_i$ 
17: end procedure

```

is larger than the maximal factor of c , and a given prime p_S . The elements of P_S are called *small sieving primes*. We say that a prime p is a *large sieving prime* if $p_S < p \leq p_S^2$ holds.

In our project by **sieving** we mean a method which eliminates the elements from H which generate numbers having a prime factor up to $p_M \approx p_S^2$. The exact description of this method can be found in [subsection 3.3](#).

We have to point out that the more than 2000 years old method called *sieve of Eratosthenes* is still a cutting edge tool for finding all prime numbers up to a given bound even in 2020. Of course, a time-efficient implementation is necessary. For example, the program run in the *Cc22 – project* produced and stored in an array the primes up to $p_S = 134\,217\,689 \approx 2^{27}$ in less than 5 seconds.

3.3. The details of the sieving method

As a matter of fact the our sieving is a simple variant of the generalized sieve with some linear polynomials $f_i(x)$ where $i = 1, 2, \dots, k$.

If we set the parameters correctly, then for every $p > p_k$ the linear congruence $f_i(x) \equiv 0 \pmod{p}$ must have exactly one incongruent solution, which is denoted by h . It is clear that the numbers $h, h + p, h + 2p, \dots \in H$ generate numbers having a prime factor p . Now we can say that “we sieve H with p ”, i.e. we remove the set $\{h, h + p, h + 2p, \dots\}$ from H . Naturally, each sieving prime can sieve at most k -times. In practice, we defined an array B such that the elements of H are the indexes of B . Every value in B is initially 1. If we find that any $f_i(h)$ has a prime factor in P_S for an $h < |H|$, we change the values $B[h], B[h + p], B[h + 2p], \dots, B[h + qp]$ to 0, for all $h + pq < |H|$. The sieve with small primes can be carried out easily on one fast processor with large operative memory, but the large prime sieve needs numerous processors and threads. In order to be able to continue the sieving on lower performance computers, we store the indexes of the 0 elements into an array A . A is about 30 times smaller than B , so we can take advantage of the cache memory and we can make the parallelization of the further sieving even with lower-capacity processors.

Now assume that we have a multiprocessor computer or a grid and we can simultaneously use n threads and let us consider the set of large primes, i. e. $P_L = \{p \in \mathcal{P} \wedge p_S < p < p_S^2\}$, where \mathcal{P}

denotes the set of prime numbers. Every thread receives a copy of A , a lower and an upper bound from the interval $(p_S, p_S^2]$. Denote by A_i the copy of A received by the i th thread ($1 \leq i \leq n$). Then every thread performs a sieving process from the given lower bound to the upper bound, producing an array of primes, a so called prime sieve table. Then the thread sieves its own copy of A with the primes found in its own prime sieve table. In this stage the effect of sieving on the set A can be described by the following command:

$$A := A \setminus \{h, h + p, h + 2p, \dots, h + qp \mid q \in \mathbb{N}, h + qp \leq |H|\}.$$

After the i th thread finished sieving with all primes in its prime sieve table, A will be updated which means that we remove all numbers x from A for which $x \notin A_i$. Then if necessary the prime sieve table will be refilled by large primes and the sieving of the updated A_i may be restarted.

We stop sieving if our program completes the sieving for all primes $p \leq p_S^2$. Finally, the output set (or vector) \bar{A} contains numbers which have not prime factors less than p_S^2 . The pseudocode of our complete sieving method can be seen in [Algorithm 2](#) and [Algorithm 3](#).

4. Conclusions

As the test results our programs show, in the nearly future an effective implementation of the probability primality tests combined our newly designed “generalized sieve algorithm” would be an appropriate tool for investigating large “curious prime combinations”.

5. Acknowledgement

The project has been supported by the European Union, cofinanced by the European Social Fund, EFOP-3.6.1.-16-2016-0023.

6. References

- [1] S. Yates, *Titanic primes*, Journal of Recreational Mathematics 16(4), 1984, pp. 250-262.
- [2] C.K. Caldwell, *The Prime Pages*, 2020, [url](#)
- [3] S.Y. Yan, *Computational Number Theory and Modern Cryptography*, Higher Education Press, 2013, ISBN 978-1-118-18858-3
- [4] P. Ribenboim, *The Little Book of Bigger Primes*, Springer, 2004, ISBN 0-387-20169-6
- [5] H. Riesel, *Lucasian Criteria for the Primality of $N = h \cdot 2^n - 1$* , Math. Comp. 23, 1969, pp. 869-875. [CrossRef](#)
- [6] G. Farkas, *Quadratic Fields from Mathematics and Informatics Point of View, Habilitation Thesis*, ELTE-IK Budapest, 2012, 109 p.
- [7] V. Shoup, *A Computational Introduction to Number Theory and Algebra*, Cambridge University Press, 2008, [CrossRef](#)
- [8] K.H. Indlekofer - A. Járαι, *Largest Known Twin Primes and Sophie Germain Primes*, Mathematics of Computation 68(227), 1999, pp. 1317-1324. [CrossRef](#)
- [9] G. Farkas, G. Gévay, P. Magyar, B. Szekeres, *Járαι’s Prime Hunting Method Reloaded (The Largest Known Cunningham Chain of Length 2 of the 2nd Kind)*, Annales Univ. Sci. Budapest, Sect. Comp. 50, 2020, accepted.

- [10] K.H. Indlekofer - A. Járαι, *Largest Known Twin Primes*, Mathematics of Computation 65, 1996, pp. 427-428. [CrossRef](#)
- [11] T. Csajbók, G. Farkas, A. Járαι, Z. Járαι, J. Kasza, *Report on the largest known twin primes*, Annales Univ. Sci. Budapest, Sect. Comp. 25, 2005, pp. 247-248.
- [12] T. Csajbók, G. Farkas, A. Járαι, Z. Járαι, J. Kasza, *The largest known twin primes of the World*, $16869987339975 \cdot 2^{171960} \pm 1$ (51779 digits), 2005, [url](#)
- [13] T. Csajbók, G. Farkas, A. Járαι, Z. Járαι, J. Kasza, *Report on the largest known Sophie Germain and twin primes*, Annales Univ. Sci. Budapest, Sect. Comp. 26, 2006, pp. 181-183.
- [14] T. Csajbók, G. Farkas, A. Járαι, Z. Járαι, J. Kasza, *The largest known twin primes of the World*, $100314512544015 \cdot 2^{171960} \pm 1$ (51780 digits), 2006, [url](#)
- [15] T. Csajbók, G. Farkas, A. Járαι, Z. Járαι, J. Kasza, *The largest known Sophie Germain prime of the World*, $137211941292195 \cdot 2^{171960} - 1$ (51780 digits), 2006, [url](#)
- [16] T. Csajbók, G. Farkas, A. Járαι, Z. Járαι, J. Kasza, *The largest known twin primes of the World*, $194772106074315 \cdot 2^{171960} \pm 1$ (51780 digits), 2007, [url](#)
- [17] T. Csajbók, G. Farkas, A. Járαι, Z. Járαι, J. Kasza, *The largest known Sophie Germain prime of the World*, $620366307356565 \cdot 2^{253824} - 1$ (76424 digits), 2009, [url](#)
- [18] T. Csajbók, G. Farkas, A. Járαι, Z. Járαι, J. Kasza, *The largest known Sophie Germain prime of the World*, $648621027630345 \cdot 2^{253824} - 1$ (76424 digits), 2009, [url](#)
- [19] G. Farkas, G. Gévay, A. Járαι, E. Vatai, *The largest known Cunningham chain of length 3 of the first kind*, Studia Universitatis Babes-Bolyai Mathematica 59(4), 2014, pp. 457-462.
- [20] A. Járαι, *World Records in Computational Number Theory*, [url](#)
- [21] A. Járαι, *Számítógépes számelmélet*, 2009, [url](#)
- [22] P.T. Bateman, R.A. Horn, *A heuristic asymptotic formula concerning the distribution of prime numbers*, Mathematics of Computation 16(79), 1962, pp. 363-367. [CrossRef](#)
- [23] T. Csajbók, G. Farkas, J. Kasza, *Sieving for Large Twin Primes and Cunningham chains of length 2 of the second kind*, Annales Univ. Sci. Budapest, Sect. Comp. 38, 2012, pp. 117-128.
- [24] G. Farkas, E. Vatai, *Sieving for Large Cunningham Chains of Length 3 of the First Kind*, Annales Univ. Sci. Budapest, Sect. Comp. 40, 2013, pp. 215-222.

PERFORMANCE OF CELL PHONE CONTROLLED MODEL VEHICLE

János Hegedűs-Kuti^{a*}, Mátyás Andó^b

^a ELTE, Faculty of Informatics, Savaria Institute of Technology, engineer instructor

^b ELTE, Faculty of Informatics, Savaria Institute of Technology, associate professor

ABSTRACT

The objective of the project was to construct a model car - with using additive technology - which is connected to a phone via wireless communication. PLA (Poly-Lactic Acid) was used as a material to print the units. The total weight of the model car is 690 grams including the electronic components. The power consumption and driving properties were measured under given circumstances. Based on our calculations, even in active use at its maximum speed of 5.16 km/h, the system is capable of at least 3.9 hours of operation, while full charging takes only 3 hours. Consequently the model vehicle can be continuously operated by applying two battery units.

Keywords: *3D printing, Arduino, driving properties, FDM/FFF, operating schedule*

1. Introduction

Nowadays, one of the most dynamically evolving technologies is the layer-by-layer manufacturing procedure. Due to the high level of flexibility of the additive manufacturing technology, the number of customized parts increase and at the same time, the quantity of materials used in production decreases. The essence of fused deposition manufacturing procedure is that the material thread – available in diverse form of plastic filaments – is transmitted by a motor to the programmed place through a nozzle. In the nozzle the plastic filament melts at high temperature, and when it gets to the print bed it quickly cools down and solidifies. This is how the product is formed layer-by-layer [1, 2].

Unlike traditional industrial technologies, in additive production the object is fabricated layer upon layer, through a method in which tiny elements (particles, filaments) are melted together. Due to the appropriate material and mechanical properties of 3D printing, its scope of usage has widely extended from producing prototypes. Parts printed in different layer structures show different mechanical properties [2]. There are two structures: in the first structure one layer is equal to the longitudinal axis of the test object, and the other one is applied perpendicularly. This is called 90° orientation. In the second structure, the first layer is at 45°, and the second one is also applied perpendicularly, this is called 45° orientation [3]. FDM (Fused Deposition Modelling) or FFF (Fused Filament Fabrication) are the most common technologies in Hungary [4], as they have a wide spectrum in the quality and pricing of printed goods. The two most popular materials of 3D technology are ABS (Acrylonitrile butadiene styrene) and PLA [5].

Other significant example for the increasing popularity of these new technologies is the expanding use of microcontrollers. As a result, the main control panel of the model car is an Atmel ATmega328P microcontroller card which is a sole microcontroller integrated into a chip. This contains the pro-

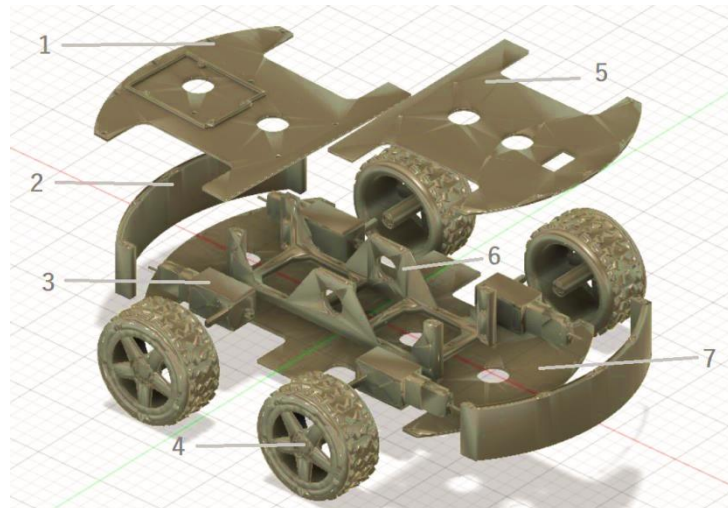


Figure 1. Main components of the model vehicle

cessor, the memory and the Arduino Uno I/O controller. The great advantage of microcontrollers is that they can be generally used both in controlling and regulating tasks. It supports open source hardware and open source software, is freely programmable, making it ideal for development environments, widespread due to its low cost and easy connectivity to other devices [6]. Programs can be uploaded to the machine via USB. In self-driving car researches they are used more and more frequently as sensors can be easily connected to the programmable motherboard. It is able to follow e.g. drawn lines (Fuzzy logic) [7] when it is connected to infrared sensors and using algorithms.

Aim of our work was the design and performance analysis of a cell phone controlled model vehicle. The vehicle was manufactured by 3D printing and it was driven by a commercial cell phone through an Atmel ATmega328P microcontroller. Energy consumption of the vehicle was monitored and optimized by operating time tests.

2. Materials and methodology

2.1. Raw materials and methodology

The printed parts of the car are made of ABS (Prusamet ABS, Pruse Research) and PLA (Prusament PLA, Prusa Polymers) materials with FDM technology. The printing was carried out with the Prusa i3 mk3S 3D printer. The parts of the model car are the followings: the roof elements (1 and 5), bumper (2), four DC motors (3), running gear (6) chassis (7), the Atmel ATmega328P microcontroller, Arduino L293D Sensor Shield DC motor controller, a HC-05 Bluetooth modul and two ICR18650 Samsung 3000 mAh rechargeable battery cells in serial connection (Fig. 1).

Table 1. Recommended printing settings and mechanical characteristics from data

	ABS	PLA
Printing temperature [°C]	260	210
Temperature of the print bed [°C]	110	40-60
Printing speed [mm/s]	40-200	40-200
Tensile rigidity [MPa]	42	50.8
Tensile modulus [GPa]	1.6	2.2

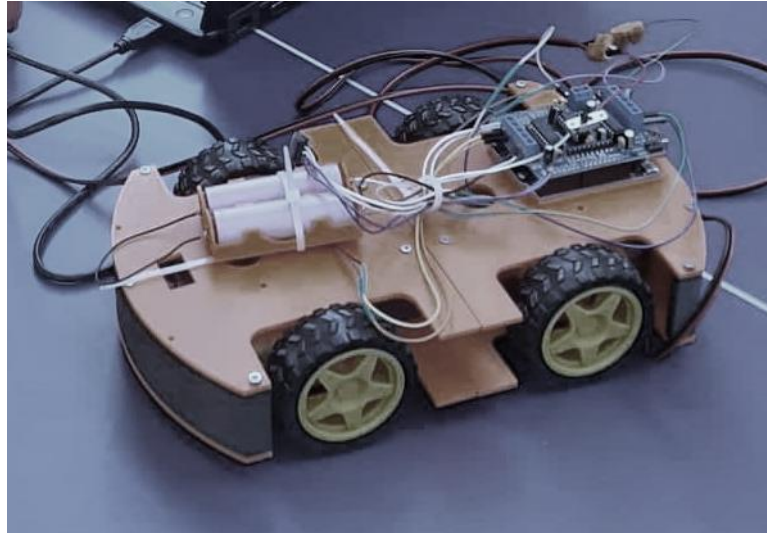


Figure 2. The assembled model car

2.2. Printing issues and solutions

For the first printing ABS were applied (main characteristics are in the [Table 1](#)), with 0.2 mm layer thickness and 250 °C printing temperature, 110 °C printing bed, 45° orientation. During the printing, it was experienced that in some cases the first layer did not stick to the print bed sufficiently, which caused the moving of the model and its separation from the print bed. To avoid this problem, the distance between the nozzle and the built plate was recalibrated. Another problem we faced during the assembly was strength issues; due to this the parts snapped and broke when we tightened the screws. The strength problem was solved by changing the material and analyzing the relationship between the printing parameters and the mechanical properties. In order to achieve ideal strength, Prusament PLA Galaxy Black material in 1.2 mm diameter [8] was used instead of ABS and the printing parameters were determined based on the literature [9]: 20% material fill, 45° orientation, 40 mm/s printing speed and 205 °C printing temperature. It must be noted that based on [Table 1](#) the higher printing temperature should increase the stiffness, however the ultimate temperature recommended by the manufacturer (205 °C) were maintained. The assembled model car can be seen on [Fig. 2](#). It weighs 690 g.

2.3. Characteristics of the electric system

The electric system of the car ([Fig. 3](#)) was designed to four-wheel drive (4WD), so all four wheels are directly driven. When the car turns, the wheels on one side rotate in one direction while the wheels on the other side rotate in the opposite direction.

The tests were carried out on a Samsung A40 smart phone with Android 10 operating system, which communicates with the motor control unit with Bluetooth. The program uploaded to the device was developed in Arduino 1.8.12 environment.

Having Arduino Bluetooth RC Car application downloaded, the Bluetooth connection was established without error. Only one device is allowed to connect at a time. The communication between the cell phone and the vehicle was stable and smooth during the tests. On the basis of the testing, the system worked without reception problems in open space in a 60 m range and it reacted directly for the control even from the farthest point. There were no tests carried out for longer ranges in the situations emerging later. Technical requirements concerning control were shaped by developing the target program. Theoretically, the basis of the solution is the following: by using Master (cell phone)

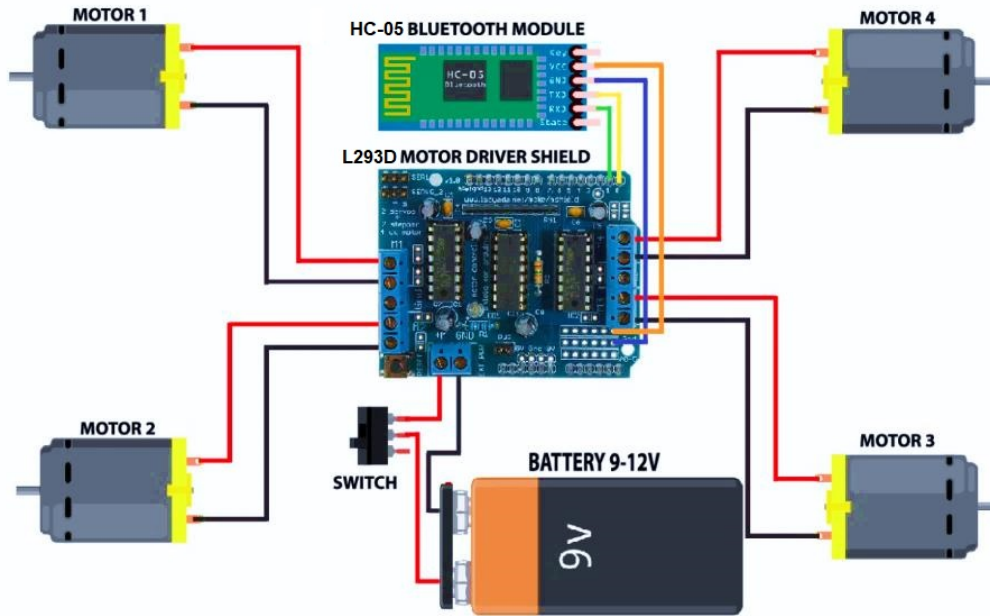


Figure 3. Circuit diagram

– Slave (model car) connection. The values of X and Y axes sent from the virtual joystick which control the speed of the motors, have to be read and sent to Slave side. The analogue values of the joysticks (0-1023) have to be converted first to the range of 0-255 (1 byte) as 4 bytes would cause a significant delay in controlling. After sending the steering command, we should read out these values through the microcontroller.

If the joystick stands in the middle, there is no movement, the car is standing. To move forward and backward, the values of axle Y are used and to move to the right or to the left, the values of axle X are used. When turning to the right, performance of the left side motor was reduced, and right side performance was increased. Turning to the left, it is the other way round. The wheel-base of the vehicle is 125 mm, the track is also 125 mm, and thanks to the all-wheel drive, the turning radius of the car is minimal, only 140 mm, in spite the fact that the wheels cannot be steered.

2.4. Measurements of power consumption

Power consumption was measured by a Maxwell Mx 25328 digital multimeter connected to the computer via USB. The tests were carried out on a flat ground with a fully charged battery, and experienced no voltage drop or any decline in the driving behavior.

For operating time test, the track was determined based on preliminary experiments. The measurement was carried out on a rectangular 10 m long and 1 m wide track, with semicircles with a radius of 0.5 m at the edges of the rectangle (Fig. 4). The measurements were carried out on a straight and smooth ground, the progress, deceleration and then turning of a vehicle accelerating from a standing position to a maximum speed and then maintaining this speed. One measurement lasted for two laps on the track, with running out of the track at the end of the second lap. This was repeated four times.

Further tests were carried out to determine the maximal speed, where the time was measured to take 10 meters. The test were repeated six times then the average lap time was calculated to determine the maximal speed.

Table 2. Power consumption values

	$I_{i,average}$ [A]	$I_{i,max}$ [A]	$I_{str,average}$ [A]	$I_{rad,average}$ [A]	Time [s]
Meas. Lap 1,	0.8384	1.45	0.7524	0.9906	43
Meas. Lap 1,	0.8336	1.60	0.7665	0.9244	41
Meas. Lap 2,	0.8277	1.42	0.7494	0.9876	42
Meas. Lap 2,	0.8241	1.49	0.7455	0.9143	40
Meas. Lap 3,	0.8019	1.51	0.7281	0.9771	41
Meas. Lap 3,	0.8192	1.41	0.7336	0.9511	42
Meas. Lap 4,	0.8073	1.41	0.7199	0.9665	40
Meas. Lap 4,	0.7973	1.37	0.7135	0.9607	42

3. Results

To define the potential operation time, power consumption tests were conducted on the track (Fig. 5). The measurements were taken 0.5 s. Based on this, the power consumption was calculated by the following formula:

$$I_{i,average} = \frac{\sum_{i=0}^n I_i}{n}, \tag{1}$$

where i represents the number of the measurement and n refers to the number of data registered during each measurement. From each lap the maximum value ($I_{i,max}$) was selected then the necessary time to take a lap was defined. The results are shown in Table 2. Further tests were carried out at standing position, in which the model car showed 0.046 A consumption, increasing to 0.056 after connected to Bluetooth. Analyzing how each lap starts, it shows that following the first acceleration, there is a local peak power consumption at 0.9 A. Subsequently the straight run when the car reached its top speed, where the power consumption is slightly higher than at the first straight run of each test with almost 0.8 A. The following straight runs showed values close to 0.7 A.

It is obvious that the maximal power consumption was observed at the curves of the lap. The peak value depends on the time when the test was taken and the highest consumption is above 1.6 A. Based on the maximum values, it is visible that the average peak values show minimal differences at the turns. It is also clear that the power consumption portrays the same image at each turn. Due to the turning, the movement of the wheels is not continuous - they stop and then start (accelerate) again – that is why both maximum and minimum values are present at each turn. The standard

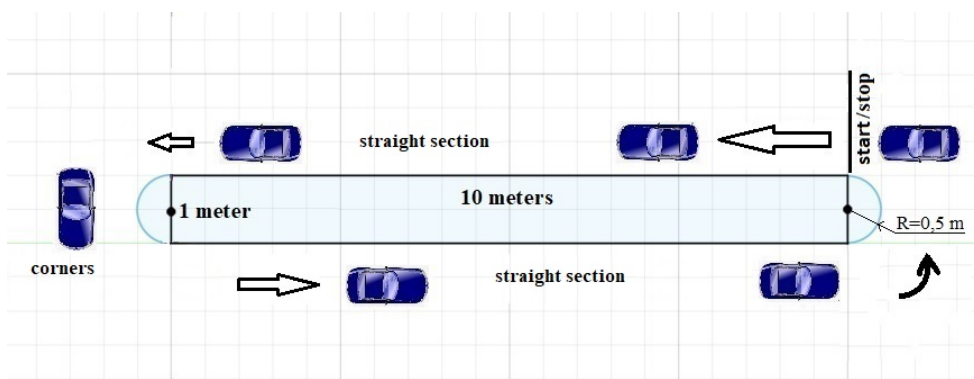


Figure 4. The track used to analyze the operating time

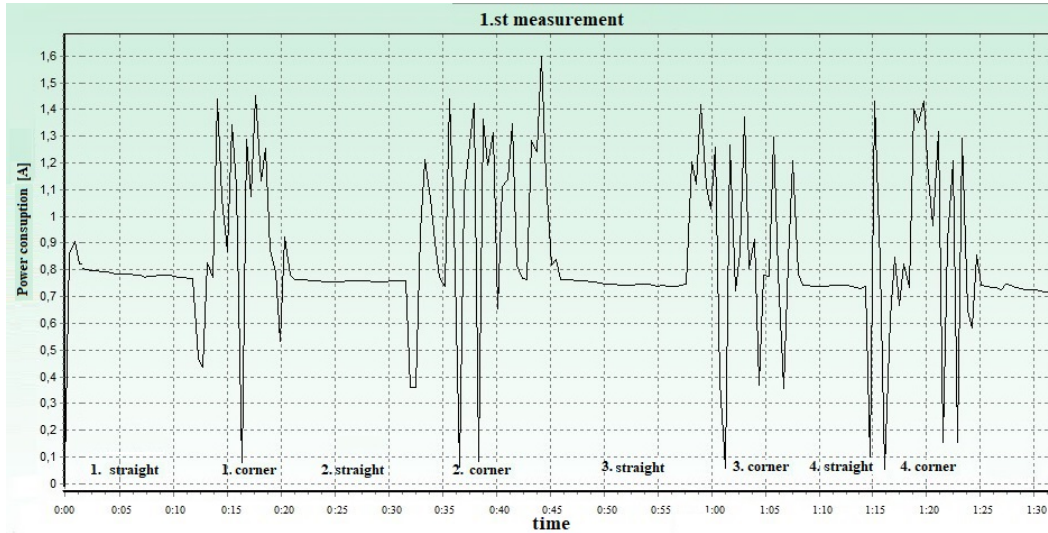


Figure 5. The results of the measurements

deviation of the lap times were small in the measurements, as a result, the testing conditions are comparable. Based on the power consumption data the operation time can be defined:

$$t_i = \frac{Q}{I_{i,average}}, \quad (2)$$

where t represents operation time [h], Q the capacity of the battery cells [mAh] and $I_{i,average}$ [A] refers the average of power consumption during measured during the tests. Based on the tests, the two 3000 mAh battery can guarantee 3.9 – 4.2 hours of operation time in continuous use. In the meanwhile, the XTAR MC4 4-slot charger can recharge the batteries in 3 hours using 1 A charging current. It means that the continuous use can be guaranteed with 2x2 batteries. The measured current is the current consumption of the entire vehicle including the microcontroller and the bluetooth module. There are two driver IC-s so the measured current goes through two different IC hence the load is acceptable without heatsink.

4. Summary

A cell phone controlled unique model car was developed, which can be used for vehicle simulation tests or to perform various logistic tasks. The model is based on a relatively cheap and available 3D printing technology. To ensure necessary stiffness of the vehicle's body, PLA material was used by considering the recommended technological parameters: 20% material fill, 45° orientation, 40 mm/s printing speed and 205 °C printing temperature. The established Bluetooth connection worked smooth without problems during the tests, consequently a cell phone can be used to remote control a vehicle. Maximum speed of the model car was 5.6 km/h, and the batteries ensured 3.9 hour operation time while the charging time was 3 hours. While turning, a significant slip can be experienced as the wheels on the two sides are capable for turning in reverse directions, too. Accordingly, the turning radius became 140 mm.

5. References

- [1] M.W. Barclift, C.B. Williams, *Examining variability in the mechanical properties of parts manufactured via polyjet direct 3D printing*, 23rd Annual International Solid Freeform Fabrication Symposium - An Additive Manufacturing Conference, 2012, pp. 876-90.

- [2] B.K. Dong, H.L. In, Y.C. Hae, *A study on mechanical properties of additive manufactured polymer materials*, Transactions of the Korean Society of Mechanical Engineers 39, 2015, pp. 773-80. [CrossRef](#)
- [3] V. Vega, J. Clements, T. Lam, A. Abad, *The effect of layer orientation on the mechanical properties and microstructure of a polymer*, Journal of Materials Engineering and Performance 20, 2011, pp. 978–88. [CrossRef](#)
- [4] *Polimer termékek kisszériás gyártása, Jegyzet*, Budapesti Műszaki és Gazdaságtudományi Egyetem Gépészmérnöki Kar Polimertechnika Tanszék, 2017, [url](#)
- [5] FreeDee Blog, *PLA vagy ABS? Ez itt a kérdés!*, visited 28.04.2014, [url](#)
- [6] G. Ruzsinszki, *Mikrovezérlős Rendszerfejlesztés C/C++ nyelven I.*, Creative Commons (CC BY-SA 2.5), 2013, ISBN 978-963-08-7260-7, pp. 67-76.
- [7] L. Gál, B. Könczöl, *Fuzzy logikát alkalmazó, vonalkövető autó viselkedésének vizsgálata*, Mérnöki és Informatikai Megoldások|Engineering and IT Solutions I., 2020, pp. 40-47. [CrossRef](#)
- [8] Shop.prusa.3d.com, *Prusament PLA Jet Black 1kg*, visited: 29.04.2020, [url](#)
- [9] B. Ádám, B. Polgár, *3D nyomtatott próbatestek mechanikai vizsgálata*, Gradus 6(1), 2019, pp. 185-191, ISSN 2064-814, [url](#)

ANALYSING FUZZY LOGIC-BASED LINE FOLLOWING MODEL CAR

Boldizsár Könczöl^a, László Gál^{b*}

^a ELTE, Faculty of Informatics, Computer Scientist MSc, 1. year

^b ELTE, Faculty of Informatics, Savaria Institute of Technology, associate professor

ABSTRACT

In our previous work a fuzzy logic-based controller was successfully applied to a line following model car utilizing Arduino Uno. Regarding fuzzy operations (t-norms), this logic has several implementations and our aim was to show how functional can be the chosen ones, and whether there are any remarkable differences among them. The fuzzy rules were very easy to create, except the drastic t-norm, all of them completed the tests, thus it can be stated that using fuzzy logic is convenient for line following. In this paper we focus on the impact of using a more capable microcontroller (Espressif ESP32) based board for the controller. Improvement of results is expected because of the higher computing performance of this board.

Keywords: *fuzzy, Arduino, microcontroller, line following*

1. Introduction

Nowadays, self-driving cars became important, because they can navigate themselves without the driver's intervention. These cars have multiple sensors and cameras, which use different algorithms to analyze situations during driving and endeavor to make the right decision, while these take a huge amount of input signals and information into account. The classical Boolean algebra, the bivalent (binary) logic, is not effective for situations like this. There are several ways to implement not only bivalent logic but also polyvalent logic, for which fuzzy logic is an excellent example. It is made for giving back a value depending on multiple inputs or using these to send a signal to the controller output. It can be also calculated with using a gradually overlapping rulebase. Initially, the western countries thought that fuzzy logic is not suitable for practical applications, but on the contrary, eastern countries, especially the Japanese, were thinking the opposite way. They successfully simulated the use of fuzzy logic in railway transport in Senda, then they turned this simulation real in 1987 [1]. Today the system of fuzzy logic is capable of being used in different artificial intelligences, self-driving systems and of acting like human (or better than human) for several kinds of traffic situations. The everyday usage of fuzzy logic is not newfangled. This could be a surprise, but almost everyone used the concept of fuzzy, when for example say freezing, cold, warm, hot, burning for some objects. Using two different type of programmable microcontroller boards (Arduino Uno, ESP32 devkit v1) and some sensors connected to them a model car was built. This model car is capable of following the line drawn by the user. For decision-making procedure, the car uses fuzzy logic, fuzzy operations (t-norms), thus a fuzzy inference system was implemented. Furthermore, there is an interesting aspect in using fuzzy logic: it could be implemented by adapting different t-norms. Finally, during the comparison of test results, it was analysed that which t-norm

is more useful for line following or whether there are any improvements using ESP32 based board instead of Arduino Uno.

2. Methods

2.1. Fuzzy logic basics

To understand fuzzy sets, the knowledge of the classical set theory definitions and attributes could be useful. To distinguish these theories, the classical, non-fuzzy sets are called crisp sets. Definitions:

- Membership function: for any set X , a membership function on X is any function from X to the real unit interval $[0,1]$.
- Fuzzy set: a fuzzy set is a pair (U, m) where U is a set and $m : U \mapsto [0,1]$ a membership function [2].
- Membership value/degree: For an element x of X , the value $\mu_A(x)$ is called membership degree of x in the fuzzy set A .
- Support: $S(A) = Supp(A) = A^{>0} = x \in U | m(x) > 0$ is called support.
- Core: $C(A) = Core(A) = A^{=1} = x \in U | m(x) = 1$ is called core.
- Height: the supremum of a fuzzy set's values: $h(A) = sup_{x \in X} A(x)$.

2.2. Operations

Two of the three main operations (intersection, union, negation) are different from the classical (crisp) set operations. In fuzzy set theory there are multiple interpretations. The standards are Zadeh's operations [3].

- Intersection (t-norm): $(A \cap B)(x) = \min[A(x), B(x)]$.
- Union (t-conorm): $(A \cup B)(x) = \max[A(x), B(x)]$.
- Standard negation: $\bar{A}(x) = 1 - A(x)$.

The intersection and union operations are associative and could be extended for unlimited number of fuzzy sets. This attribute is truly important, because in this project 3 inputs were analysed, thus we had to exploit this property on each t-norm. The union operation (t-conorm) was not used, but 6 well known or promising t-norms were tested in this application. The basic properties of these t-norms could be seen in following subsection.

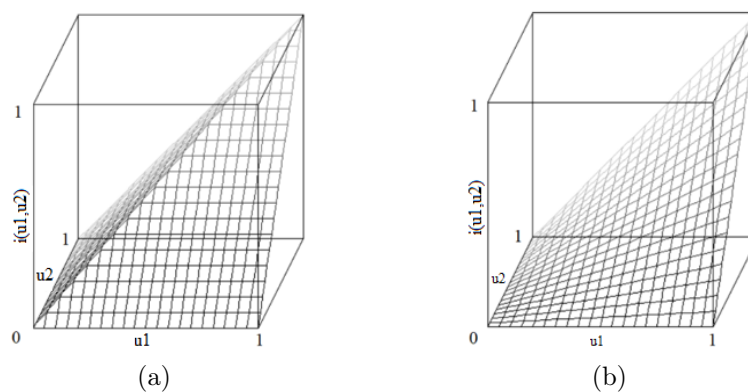


Figure 1. a) Graph of the minimum (standard) t-norm [4], b) Graph of the algebraic product t-norm [4]

2.3. Used t-norms

1. Standard (minimum) t-norm

The minimum t-norm, as its name suggests, gives the minimum of the input values as output value (Fig. 1(a)). μ_1 and μ_2 are fuzzy membership values calculated from the two inputs (e.g. sensor values) using fuzzy membership functions:

$$w_m = \min(\mu_1, \mu_2). \quad (1)$$

For three inputs:

$$w_m = \min(\mu_1, \mu_2, \mu_3). \quad (2)$$

2. Algebraic (product) t-norm

The second test is on the algebraic product t-norm. The output is the product of input values (Fig. 1(b)):

$$w_a = \mu_1 \cdot \mu_2. \quad (3)$$

For three inputs:

$$w_a = \mu_1 \cdot \mu_2 \cdot \mu_3. \quad (4)$$

3. Drastic t-norm

An extremist t-norm, the output differs from zero only where at least one of the inputs is 1 (Fig. 2(a)). Due to its drastic behavior, difficulties were expected in applying this one for line following.

$$w_d = \begin{cases} \mu_1, & \text{if } \mu_2 = 1; \\ \mu_2, & \text{if } \mu_1 = 1; \\ 0, & \text{otherwise.} \end{cases} \quad (5)$$

For three inputs:

$$w_d = \begin{cases} \mu_1, & \text{if } \mu_2 = 1 \text{ és } \mu_3 = 1; \\ \mu_2, & \text{if } \mu_1 = 1 \text{ és } \mu_3 = 1; \\ \mu_3, & \text{if } \mu_1 = 1 \text{ és } \mu_2 = 1; \\ 0 & \text{otherwise.} \end{cases} \quad (6)$$

4. Łukasiewicz

Jan Łukasiewicz, polish mathematician's t-norm (Fig. 2(b)):

$$w_L = \max(0, \mu_1 + \mu_2 - 1). \quad (7)$$

For three inputs:

$$w_L = \max(0, \max(0, \mu_1 + \mu_2 - 1) + \mu_3 - 1). \quad (8)$$

5. Trigonometric

A "smooth" t-norm based on trigonometric functions (Fig. 3(a)) [5]:

$$w_t = \frac{2}{\pi} \arcsin \left(\sin \left(\mu_1 \frac{\pi}{2} \right) \cdot \sin \left(\mu_2 \frac{\pi}{2} \right) \right). \quad (9)$$

For three inputs:

$$w_t = \frac{2}{\pi} \arcsin \left(\sin \left(\mu_1 \frac{\pi}{2} \right) \cdot \sin \left(\mu_2 \frac{\pi}{2} \right) \cdot \sin \left(\mu_3 \frac{\pi}{2} \right) \right). \quad (10)$$

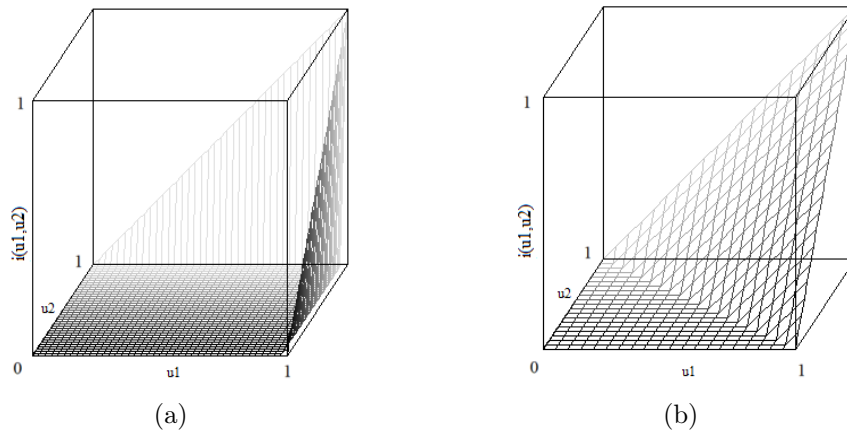


Figure 2. a) Graph of the drastic t-norm, b) Graph of the Łukasiewicz t-norm [4]

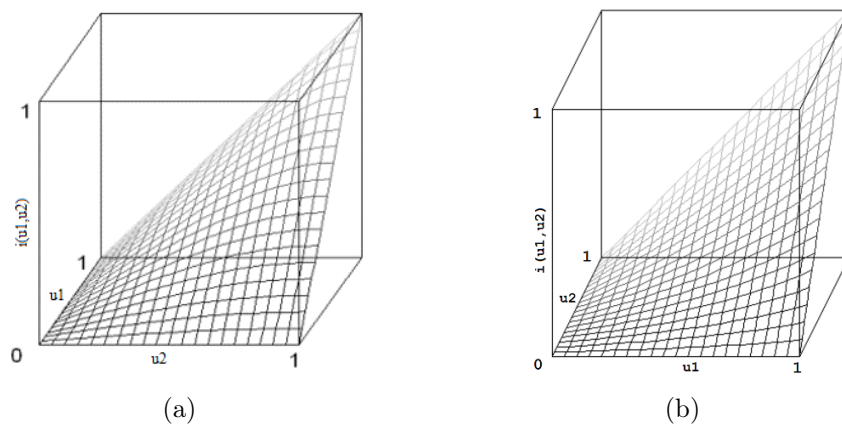


Figure 3. a) Graph of the trigonometric t-norm [5], b) Graph of the Hamacher product t-norm [4]

6. *Hamacher*

The Hamacher t-norm has a parameter (ν), a specific variant of it ($\nu = 0$) is the Hamacher product t-norm (Fig. 3(b)):

$$w_H = \frac{\mu_1 \cdot \mu_2}{\mu_1 + \mu_2 - \mu_1 \cdot \mu_2}. \tag{11}$$

For three inputs:

$$w_H = \frac{\mu_1 \cdot \mu_2 \cdot \mu_3}{\mu_1 \cdot \mu_2 + \mu_1 \cdot \mu_3 + \mu_2 \cdot \mu_3 - 2 \cdot \mu_1 \cdot \mu_2 \cdot \mu_3}. \tag{12}$$

3. Hardware setup

3.1. Main parts

1. Computing boards:

Two different mainboards were used for the tests. The first was the quasi standard low-cost development board – Arduino Uno. The counterpart was an ESP32 based low-cost, Arduino IDE compatible development board with advanced performance and special features (like Wi-Fi and Bluetooth, although none of them was used for this project).

Arduino Uno (compatible) mainboard

- Atmel ATmega328P microcontroller,
- 8-bit architecture,
- 1 core,
- 16 MHz clock rate,
- 10-bit ADC,
- Arduino Sensor Shield v5.0.

ESP32 Devkit V1 mainboard

- Espressif ESP-WROOM-32 module,
- ESP32-D0WDQ6 microcontroller chip,
- 32-bit architecture,
- 2 cores,
- 240 MHz clock rate,
- 12-bit ADC.

2. L298N dual H-bridge DC motor controller.
3. 4 DC motors.
4. HC-05 (ZS-040) bluetooth module.
5. 3 MH-Sensor-Series infrared reflective sensors (with LM393 comparator).
6. The power is supplied by 3 pieces of 18650 battery cell, regulated by a DC-DC „step-down” converter module (9V stable).

ESP32 (microcontroller) based development boards are compatible with Arduino development environment (Arduino IDE), the programming language and the libraries are significantly the same for both boards. But as the specifications show us, the ESP32 is more powerful, than Arduino Uno (ATmega328P) and it has a floating-point unit while Uno not. According to these better results is expected from the ESP32, then from the Uno.

3.2. Modifications

1. *Infrared reflective modules*

After connecting the three modules, the digitized values of the analog outputs of the modules were checked with the Arduino IDE serial monitor before the real tests. These values are between 0-1023 for Arduino (10 bit ADC) and between 0-4095 for ESP32 (12 bit ADC). There were huge differences between the infra sensors' values. The main reason for that was the difference in the (infra) LED light intensity of the modules. It could be easily checked this through a smartphone camera. Checking the sensors and their datasheets, to following conclusion was realised: the problem could be solved by changing the SMD resistors to variable ones (multi turn trimpot, trimmer). For safety, a 150 Ω resistor was connected in series for each trimmer. Because of the different required voltage level of the different boards (5V for Arduino Uno, 3.3V for ESP32), it was necessary to recalibrate the sensors for each mainboard.

2. Power supply

The original power supply consisted of 4 pieces of AA batteries, but with these the speed control is very limited because of the 6/5.6 V voltage. These values are nominal battery output voltage, until this voltage reaches the motors, it goes through different electronic parts, so ca. 5.4/5 V usable voltage reaches the motors. Therefore, instead of this, 3 pieces of 18650 Lithium-ion batteries were used. Due to these batteries, the voltage is between 10.1 V and 12.6 V, which is more than enough. Contrary to this, the charging level changes results, so a DC-DC step-down module is connected to this pack of batteries. The output voltage was set to 9 V, so that the battery lasts longer, and the results will be consistent and easily comparable.

4. Results

The track was on a whiteboard and there were no crossroads. The car must have taken 3 full laps on the track. The time was measured with a stopwatch and from flying start, with an estimated precision of 0.1 s. In every case 3 measurements were carried out, and the median of these were compared. The results can be seen [Table 1](#) and [Table 2](#).

A Mamdani type fuzzy inference system was implemented with COG (center of gravity) defuzzification. While creating the rulebase, optimization was not an intended goal. The main aim was to test whether the operation could be affected, and to what extent do the usage of different t-norms affect this operation, especially if the fuzzy rulebase was created fast by an “expert” with minimal prior knowledge. The rules were created as described hereinafter.

If the left sensor is LIGHT, the middle sensor is LIGHT and the right sensor is LIGHT then LEFT motor STOP. In short form for the left motor: If {L, L, L}, then STOP. For better transparency, the 7 rules (R1-R7) for the left motor is given in the following formulae (LIGHT=L, DARK=D):

- R1: If {L, L, L}, then STOP.
- R2: If {L, L, D}, then FORWARD_MAX.
- R3: If {L, D, D}, then FORWARD.
- R4: If {L, D, L}, then FORWARD.
- R5: If {D, D, L}, then BACKWARD.
- R6: If {D, L, L}, then BACKWARD_MAX.
- R7: If {D, D, D}, then BACKWARD_SLOWLY.

The rules for the right motor can be easily made based on these, just some swapping is needed with left and right side.

4.1. Arduino Uno test results

The L (light) and D (dark) trapezoidal shaped fuzzy membership functions [2] are implemented using the following parameters (each sensor sends analog signal converted to discrete values from 0 to 1023, the higher value is darker, these 4 values are the 4 breakpoints of the trapezoid):

$$L = \{-1, 0, 100, 700\}$$

$$D = \{100, 700, 1024, 1025\}$$

In the expression $\{a, b, c, d\}$ a and d define the support, b and c define the core for the trapezoidal shaped (height 1) fuzzy membership function. In case of $L = \{-1, 0, 100, 700\}$ it was considered that the sensor output between 0 and 100 as “definitely light”; below -1 and above 700 as “not light at all”; whereas between 100 and 700 is a linear transition from “definitely light” to “not light at all”. The higher the sensor output value, the darker the surface below.

The trapezoids, used in the consequent of the fuzzy rules, are originally set this way (range between 0 and 255, the higher value causes faster speed):

$$\begin{aligned} \text{STOP} &= \{-10, 0, 0, 10\}, \\ \text{FORWARD_MAX} &= \{60, 75, 80, 85\}, \\ \text{FORWARD} &= \{45, 55, 65, 75\}, \\ \text{BACKWARD} &= \{-80, -75, -70, -60\}, \\ \text{BACKWARD_MAX} &= \{-90, -85, -80, -70\}. \end{aligned}$$

The created rulebase's conclusions (the duty cycle of the motors: 0-255) are calibrated for a specific voltage (12 V). The value 55 is acceptable for 12 V, but this value with 6 V is not enough to start the motor. Thus, a "speed factor" value was created which scales this value (and all the other breakpoints of the consequence trapezoid), while the rulebase could stay the same.

According to the first measurements, the base "speed factor" was 1.92. After some tests it was experienced that the stable 9 V is appropriate, which has already been set in the step-down module. With this value, all the t-norms, except drastic could complete the tests. In these tests a slightly different speed factor of 2.0 was used for both mainboards. Performance of the Arduino Uno based fuzzy reasoning line follower model car was measured for each of the selected t-norms. [Table 1](#) contains the results: measured time of three consecutive laps, where the only difference among the systems was the t-norm applied in the fuzzy inference system. As it was expected, utilizing drastic t-norm was not successful, at least not with this unoptimized fuzzy rulebase. The model car was not able to properly follow the line and stopped on the {L, L, L} condition all the time.

It is worthwhile to mention that although it was expected that the trigonometric t-norm based car perform very well, it proved to be the slowest one in this test. It was about 25% slower than the remaining four. Cause of this behavior was the higher computational resource requirement, considering it utilized much more floating-point operations (and function calls). Meanwhile, the others utilized mainly integer operations, only the Hamacher product performed one floating-point division operation. Of course, the COG defuzzification method used a few FP operations for all the t-norms.

Despite, Arduino Uno stores and handles double precision FP numbers (type double, 64 bit) as single precision ones (type float, 32 bit), the difference in the required computational effort is remarkable (compared to the integer operations). This way the latency, caused by the fuzzy reasoning, may affect the overall performance negatively.

4.2. ESP32 test results

The same Arduino IDE, the default Arduino IDE settings and almost the same source code was used for the ESP32 development board. In order to adapt to the different characteristic of the ESP32's analog-to-digital converter, some trivial changes had to be made to the fuzzy rules applied

Table 1. Results using Arduino Uno

t-norm	3 laps time [s]
Minimum	34.23
Algebraic product	36.95
Drastic	-
Łukasiewicz	37.72
Trigonometric	43.99
Hamacher product	33.41

Table 2. Results using ESP32

t-norm	3 laps time [s]	Improvement [%]
Minimum	32.49	-5.1
Algebraic product	28.25	-23.5
Drastic	-	-
Łukasiewicz	27.35	-27.5
Trigonometric	27.63	-37.2
Hamacher product	30.22	-9.5

for Arduino Uno. Each sensor's output is converted to data from 0 to 4095, the higher value is darker, these 4 values are the 4 breakpoints of the trapezoid:

$$L = \{-1, 0, 396, 3135\}$$

$$D = \{396, 3135, 4096, 4097\}$$

The consequence trapezoids are the same. Performance of the ESP32 board based fuzzy reasoning line follower model car was measured for each of the selected t-norms. The same path and the same conditions were used as before (with Arduino Uno). [Table 2](#) contains the following results: measured time of three consecutive laps, where the only difference among the systems was the t-norm applied in the fuzzy inference system.

Utilizing drastic t-norm was not successful, again. However, all the other t-norms benefited from the more powerful hardware. Although, the Łukasiewicz t-norm based system gained a notable performance boost, but in case of the trigonometric t-norm based system the improvement was huge. Therefore, these became the top two finishers – head to head.

4.3. Inference times

The fuzzy inference time of the reasoning was measured in both systems (Arduino Uno and ESP32) for all the selected t-norms using the Arduino built-in function `millis()`. Measuring the time for only one reasoning would be cumbersome, it would be in the millisecond and sub-millisecond range. We decided to measure the time of 1024 reasoning for both the left and right motors. This way [Table 3](#) and [Table 4](#) show the measured time required for $2 \cdot 1024$ fuzzy inference calculations for Arduino Uno and ESP32, respectively.

Not only the results have changed and improved by a factor of 10, but the movement of the car was way smoother with ESP32 than with Arduino Uno. Reducing calculation times contributed a great deal to the smoothness of the movement. Especially the trigonometric t-norm's performance improved a lot.

Table 3. $2 \cdot 1024$ calculations (Arduino Uno)

t-norm	interference time [ms]
Minimum	3 704
Algebraic product	3 758
Drastic	3 756
Łukasiewicz	4 035
Trigonometric	11 665
Hamacher product	4 448

Table 4. $2 \cdot 1024$ calculations (ESP32)

t-norm	interference time [ms]
Minimum	367
Algebraic product	378
Drastic	321
Łukasiewicz	344
Trigonometric	1 188
Hamacher product	471

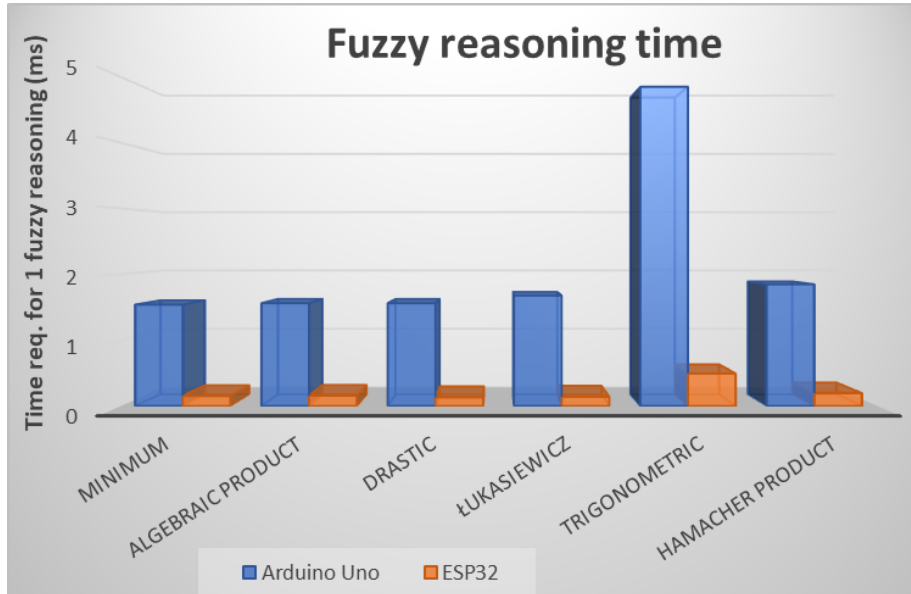


Figure 4. Time requirements for 1 fuzzy reasoning (Arduino Uno and ESP32)

4.4. Performance comparison

Fig. 4 depicts the performance improvements in the fuzzy reasoning time for different t-norms using ESP32 over Arduino Uno. Again, all the t-norm calculation times improved by approximately a factor of 10. Thus, the reasoning time moved from the millisecond to the sub-millisecond range, where the physical properties of the system (model car, mass, adhesion, DC motor inductivity) affect the performance more than the lag caused by the calculations. Therefore, the beneficial properties of a t-norm can prevail. Concerning the normalized reasoning time, the ratio among the t-norms are essentially the same (Fig. 5). While Atmel ATmega328P (Arduino UNO) does not have any floating-point unit so the FP calculations are made by software emulations, according to the specs, ESP32 does have FP units. It is a little bit disappointing to see that the FP operations performance improved only by the clock rate increasement. However, it is a bit unfair to compare these numbers because Arduino Uno handles “double” as “float”, while ESP32 handles “double” as “double” despite ESP32

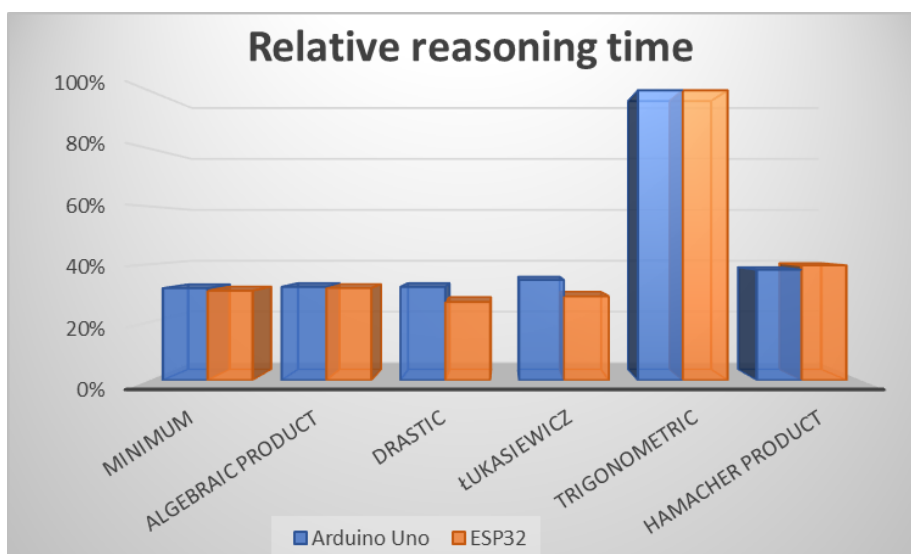


Figure 5. Normalized time requirements of fuzzy reasoning (Arduino Uno and ESP32)



Figure 6. Overall performance improvements (Arduino Uno and ESP32)

has only single precision floating point units. More calculation time improvement for trigonometric t-norm was expected, its cause can be the strange behavior of the ESP32 FP units [6].

Fig. 6 depicts the overall performance improvements due to the application of the more powerful ESP32 instead of Arduino Uno. It is evident, the trigonometric t-norm based fuzzy reasoning line following model car benefited the most from the hardware change. Being the worst one executing on Arduino Uno (by a relatively large margin) it became the best, close together with the Łukasiewicz t-norm, 27.63 s and 27.35 s respectively.

5. Conclusions

Some speed increasement for the line following model car using the ESP32 board was expected in place of the Arduino Uno because of the higher computing capabilities. It became faster than it was before, also the line following was better. The average performance improvement was 20%, it varies between 5% (minimum t-norm) and 37% (trigonometric t-norm). We expected that the trigonometric t-norm based device performs very well, compared to the other t-norms based ones due to its smooth characteristic. Nevertheless, the Arduino Uno's MCU bottleneck will really hurt its performance, eliminating this obstruction enables to unfold its potential. Using the more capable board trigonometric and Łukasiewicz t-norms became the best of the tested t-norms in terms of "speed" for line following model cars.

Although, the trigonometric calculations still needed about 3 times more time than the other t-norms despite the fact that ESP32 has a dual core CPU that is supported by floating-point unit (FPU), it acts much better on ESP32 than on Arduino Uno. Just because a microcontroller includes an FPU, it does not mean the support of all types of floating-point operations. Therefore, we intend to extend the investigation involving commonly used microcontrollers like ARM Cortex-M4 MCU (based boards), more t-norms and optimizations.

6. Acknowledgement

The project has been supported by the European Union, co-financed by the European Social Fund EFOP-3.6.1-16-2016-00023.

7. References

- [1] F. Oláh, *A Fuzzy Logika – Alapismertek*, Autótechnika 05, 2009, pp. 42-43.
- [2] Zs.Cs. Johanyák, Sz.Kovács, *A fuzzy tagsági függvény megválasztásáról*, A GAMF Közleményei, Kecskemét, XIX. évfolyam 2004, pp. 1-12.
- [3] L.T. Kóczy, D. Tikk, *Fuzzy rendszerek*, Tyoptex, 2001, p. 14.,16.,18-21.,23.
- [4] L. Gál, *Fuzzy modellek optimalizálása bakteriális típusú algoritmusokkal*, Ph.D Thesis, Győr, 2012
- [5] L. Gál, R. Lovassy, L.T. Kóczy, *Function Approximation Performance of Fuzzy Neural Networks Based on Frequently Used Fuzzy Operations and a Pair of New Trigonometric Norms*, 2010 IEEE World Congress on Computational Intelligence, WCCI-2010, Barcelona, Spain, July 18-23 (2010), pp. 1514-1521.
- [6] Espressif, *Unexpectedly low floating-point performance in C*, visited: 25.06.2020, [url](#)

ON THE SLIDING MODE CONTROL FOR PRECISION MACHINING

Luis Rubio^{a*}, Asier Ibeas^b, László E. Kollár^c

^a ELTE, Faculty of Informatics, Savaria Institute of Technology, research fellow

^b Universitat Autònoma de Barcelona, Department of Telecommunications and Systems Engineering, associate professor

^c ELTE, Faculty of Informatics, Savaria Institute of Technology, full professor

ABSTRACT

Precision machining uses linear motor actuators in order to deal with robustness and stability in the broad range of cutting conditions. Those systems are demanding more sophisticated control algorithms in order to fulfil each time more exigent tolerances in the tendency to miniaturization of products and to face more robust dynamics. Sliding mode control family is natural approach to cope with mass and damping variation and external disturbances, which are inherent characteristics of cutting processes. This paper compares conventional and super-twisting sliding mode controls on keeping the closed loop dynamics within requirements and reject disturbances created by the cutting forces.

Keywords: *precision machining, contouring control, sliding mode control, machining dynamics*

1. Introduction

Machining consists of the coordinated drive of multiple axis across rotational and linear movements. A central unit namely Computer Numerical Control (CNC) synchronizes the electric signals adequately to track as smooth as possible a predetermined tool path into a work-piece. Tool paths are generated in advance accordingly to the desired final product.

Commercial CNC provide feed forward and PID controllers as functionalities for end users to deal with transitory behaviour and steady state errors. Normally, these solutions provide enough accuracy, within tolerances, for the requirements of conventional processes. However, the current tendency to miniaturization results in unsatisfactory the achievements of these basic PID-based control schemes with feed forward compensation due to introduction of dynamic errors into the system.

High precision is required due to more sophisticated and precise tool paths, such as free form trajectories. Therefore, the motion of each machine axis needs to be controlled smoothly and precisely, so they will be able to follow the pre-programmed desired trajectory accurately according to the manufacturing machine task demand [1, 2].

The traditional approach to construct machine CNC has been to use rotary drive motors and ball-screws to achieve table motors. Linear motors offer several advantages over this approach, including low inertia, better performance, increased accuracy, and reduced complexity [3]. When using linear motors for machining, three variables must be considered, namely, mass, damping and disturbances acting on the system. The change of plant parameters results from the variations of mass of workpiece and damping due to use of lubricants. Furthermore, cutting forces are main source of disturbances in machining when linear motor actuators are used [4].

To overcome the influences of disturbances and model parameters uncertainties, natural control approach is adopted by sliding mode controller (SMC), which was first proposed by Utkin [5, 6]. These

© ELTE, Faculty of Informatics, Savaria Institute of Technology, 2020

*Corresponding author: Luis Rubio, lrr@inf.elte.hu

<https://doi.org/10.37775/EIS.2020.2.4>

controllers give some desirable closed-loop properties, including invariance, dynamic order reduction, and robustness against parameters variations and disturbances. The design of SMC consists of two stages, i.e. an equivalent control and a switching control. The equivalent control is derived from the definition of sliding surface, to which the controlled system trajectories must belong. The switching control forces the system to slide along the sliding surface despite being influenced by parameter or external disturbances.

Motion control systems become vulnerable when the output tracking signals present small oscillations of finite frequency known as *chattering*. The chattering problem is harmful because it leads to low control accuracy, and high wear of moving mechanical parts. The chattering phenomenon can be caused by the deliberate use of classical sliding mode control technique. This control technique is characterized by a discontinuous control action with an ideal infinite frequency [7]. When fast dynamics are neglected in the mathematical model, such phenomenon can appear. Another situation responsible for chattering is due to implementation issues of the sliding mode control signal in digital devices operating with a finite sampling frequency, where the switching frequency of the control signal cannot be fully implemented [7]. A solution to this problem is the high order sliding mode technique [8]. This control technique maintains the same sliding mode properties (in this sense, first-order sliding mode) with the advantage of eliminating the chattering problem due to the continuous-time nature of the control action.

In CNC machining, SMC has been applied for controlling feed drives. A SMC applied to a CNC servomechanism was presented by Eun et al. [9]. In that work, a decoupled discrete-time SMC and disturbance compensator were proposed and applied to tune the sliding mode and disturbance estimation dynamics separately. Altintas et al. [10] proposed a Sliding Mode Controller, which compensates the cutting force and pre-compensates the frictions in drives with ball screw support bearings using a model-based approach. Altintas and Okwudire [11] developed a classical sliding mode controller with cutting force recovery to achieve high bandwidth, cutting force prediction, and active compensation of structural vibrations of the machine, but the authors concluded it was not possible of practical implementation of this approach. Although chattering will lead to deteriorate machine tool and components and limits the bandwidth and setting time of the closed-loop system it has not been taken into consideration when applying SMC in machining until the publication of Xi et al's work. [12, 13]. The reasons could be explained as a lack of necessity due to that the threshold of machine performance and requirements could not be achieved at that moment. Besides, these authors presented a SMC, which incorporates an integral action in order to avoid chattering of the sliding mode control. Additionally, they proposed an approach to choose a sliding surface to influence system performance and reduce chattering. However, the integral control action just mitigates the chattering problem in certain conditions and it is not a straightforward solution. Other approaches to solve the same problem for other machining processes are well documented in the literature [14, 15].

In this paper, the third generation of sliding mode controller (SMC), namely super-twisting sliding mode control, is proposed to tackle chattering while preserving robustness against uncertainties in the drive's parameters, compensating for external disturbances and maximizing the bandwidth within physical limitations when controlling linear motors.

Chattering is proportional to the magnitude of the discontinuous control and it will affect the activity of the control action. Super-twisting SMC algorithm inherently deals with the magnitude of the discontinuous control balancing the activity of the control action. This idea supports and enhances the use of SMC in machining to deal with model uncertainties and disturbance rejection. The comparison with conventional SMC algorithm shows the benefits of applying super-twisting SMC over conventional SMC.

Super-twisting SMC control algorithm coping with high-precision machining processes was first proposed and addressed by the authors in a previous paper [16]. Later on, the work [17] applied successfully the algorithm to high precision machining in conventional processes in order to deal with friction of the process using rotatory DC motors. This study presents a comprehensive comparison of the conventional and super-twisting SMC approaches to high precision CNC machining in order to deal with the cutting forces of the process as disturbances in the micro-milling process using linear motors as drives.

The paper includes the following parts. Section 2 models the axis dynamics using linear motors for their application in machining and perturbations incurred by cutting forces. Section 3 presents conventional and super-twisting SMC algorithms. Section 4 summaries closed-loop composed by the system and the presented control algorithm. Section 5 presents simulation results, continuing with a discussion in section 6 and concluding in section 7.

2. System description

The current section introduces the modelling of linear motors impulse by direct drives. As each motor works independently, it is intended to track-control every motor independently. The model of the linear motor direct drive feed system is established according to its work principle [11, 18]. The equation, which governs the movement of the linear motor, is a second order mass-damping equation:

$$m\ddot{x} + b\dot{x} = F, \tag{1}$$

where $x = x(t)$ denotes the position and F is the external control force, m is the moving mass (table and workpiece), and b is the damping coefficient of the guide-ways, which is measured using traditional impact transient testing through a hammer or using other methods such as sweep frequency [19].

The block diagram is shown in Fig. 1 in which $1/(ms + b)$ represents the Laplace transformation of Eq. 1. The movement of a single axis of the machine tool driven by linear motor is then represented by current amplifier, motor force constant, and axis dynamics including disturbance forces. In the block diagram, $u_c(t)$, $i(t)$, $F_m(t)$ and $F_d(t)$ represents the control signal, the driven current, the force given by the linear motor and the disturbance force, respectively. The index i represents the integration step of the Eq. (1). Despite its simplicity, the model captures all the essence of the process and it is usually implemented in commercial CNCs.

One of the main sources of disturbance in machine tools driven by linear motors is given by the cutting forces. Previous studies have addressed the calculation of *cutting forces*, in which mechanistic approaches are mainly used. Different machining processes and cutting conditions lead to different

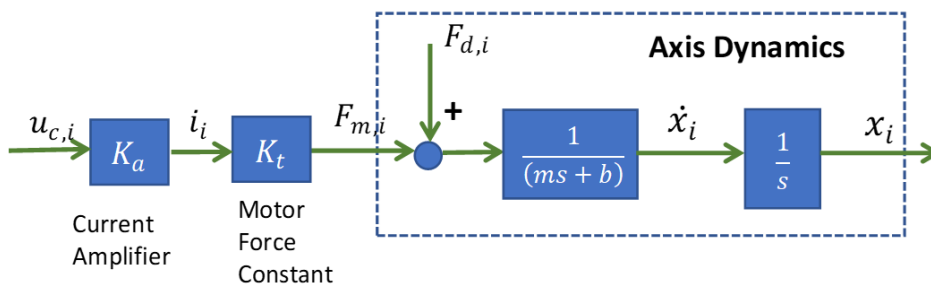


Figure 1. Block diagram of linear drive machine tool [1]

amplitudes and frequencies of the cutting process. Furthermore, low-frequency disturbances cause dynamic stiffness between the tool and workpiece, which generates vibrations. This is still an open research topic in this field [11].

3. Sliding mode control algorithm

The following sections describe the design of the controller taking as initial point the system Eq. (1) for classical SMC and super-twisting SMC with PID-type sliding surface.

3.1. Classical sliding mode control

The control signal of the SMC is normally split out into two parts, one regarding the equivalent control, which deals with the dynamics of the system and the sliding surface, and another regarding the switching control, which is responsible for keeping the dynamics of the system onto the sliding surface of the control system. So,

$$F = F^{eq} + F^{sw}. \quad (2)$$

The equivalent control F^{eq} relies on the dynamics of the system and the sliding surface, $S(t)$. The approach taken into consideration in this section is very classical and well known in the literature [7]. Consider the PID-type sliding surface:

$$S(t) = \dot{e}(t) + \mu e(t) + \lambda \int_0^t e(\tau) d\tau. \quad (3)$$

With $e(t) = x_{ref}(t) - x(t)$, and μ and λ are positive design parameters. Its time derivative is given by:

$$\dot{S}(t) = \ddot{e}(t) + \mu \dot{e}(t) + \lambda e(t). \quad (4)$$

The control gains μ and λ should be chosen so that the characteristic polynomial $s^2 + \mu s + \lambda = 0$ (s denotes a complex variable here) is strictly Hurwitz, i.e., a polynomial with roots located strictly in the open left half of the complex plane. Adequate selection of the parameters will lead to an appropriate property of the output of the system as the parameters (μ , λ) define the poles of the closed-loop system. The two parameters of the sliding surface are designed to trade-off the bandwidth of the system and noise rejection (λ [rad/s²]), and to enhance the transient response of the system (μ [rad/s]). The control objective is imposed by $\dot{S}(t) = 0, \forall t$ and $S(0) = 0$, which will give the solution of the equivalent control. Thus,

$$\dot{S}(t) = 0 = \ddot{x}_{ref}(t) - \ddot{x}(t) + \mu[\dot{x}_{ref}(t) - \dot{x}(t)] + \lambda[x_{ref}(t) - x(t)]. \quad (5)$$

Introducing Eq. (1) in Eq. (5):

$$\ddot{x}_{ref}(t) - \frac{1}{m}[F - b\dot{x}(t)] + \mu[\dot{x}_{ref}(t) - \dot{x}(t)] + \lambda[x_{ref}(t) - x(t)] = 0. \quad (6)$$

While isolated, selecting $\mu = b/m$ (bandwidth of the system), the control signal can be expressed as:

$$F = m \left[\ddot{x}_{ref}(t) + \frac{b}{m} \dot{x}_{ref}(t) + \lambda e(t) \right]. \quad (7)$$

Since the actual parameters of the system are not known, their estimates (\hat{m} , \hat{b}) must be used while, in addition, a switching term is added to cope with disturbances while driving the system into the sliding surface. Therefore, the complete sliding control law reads:

$$F = \hat{m} \left[\ddot{x}_{ref}(t) + \frac{b}{m} \dot{x}_{ref}(t) + \lambda e(t) \right] - \Lambda \text{sign}(S), \quad \Lambda > \delta, \quad \delta |S|^{1/2} > |F_d|. \quad (8)$$

The SMC algorithm guarantees the system reaches the sliding surface in some finite time. The disturbance is bounded by a finite positive scalar δ within the square root of the sliding surface, allowing the control law programming adequate Λ to track the reference signal. Programming high values of Λ introduces high frequencies to the system caused by the sign function. This element influences the control signal to be modified by chattering.

3.2. Super-twisting sliding mode control

In super-twisting algorithms [9], the switching control part allows reducing the chattering produced by high frequency signals while maintaining the main structure based basic features of the classical sliding mode controllers. In this case, the control law reads,

$$F = \hat{m} \left[\ddot{x}_{ref}(t) + \frac{b}{m} \dot{x}_{ref}(t) + \lambda e(t) \right] - \alpha \sqrt{|S(t)|} \text{sign}(S) - v(t), \quad \alpha > 0, \quad (9)$$

with $\dot{v}(t) = \beta \text{sign}(S)$, $\beta > 0$. The super-twisting SMC algorithm guarantees the system reaches the sliding surface in some finite time. The control gains (α, β) are selected such as the first time derivative of the corresponding disturbance, (\dot{F}_d) , is bounded by a finite positive scalar, γ . Basic requirement to tuning (α, β) is that $\beta > \gamma$ [7, 20] and references therein.

This controller equation guarantees the continuity of the control law and allows avoiding/reducing the chattering compared to the classical SMC algorithm. This fact leads the system to minimize tear and wear of the actuators. Moreover, control parameters can be tuned to maximize performance indexes for production requirements, such as required tolerances and production time.

It is supposed that the reference trajectories, x_{ref} , and its derivatives are known in advance since they can be obtained from the desired track and velocity requirements. With this control law, the stability of the closed loop is guaranteed in some finite time.

4. SMC algorithms schemes

Fig. 2 represents the integration of the whole control system consisting of the system dynamics including cutting forces as disturbances, and classical/conventional and super-twisting SMC algorithms. The simplicity of SMC methodologies does not require any further disturbance estimation and compensation but the intrinsically sign function to keep within the sliding surface under predefined disturbances bounds. References from required trajectories in position, velocity and acceleration

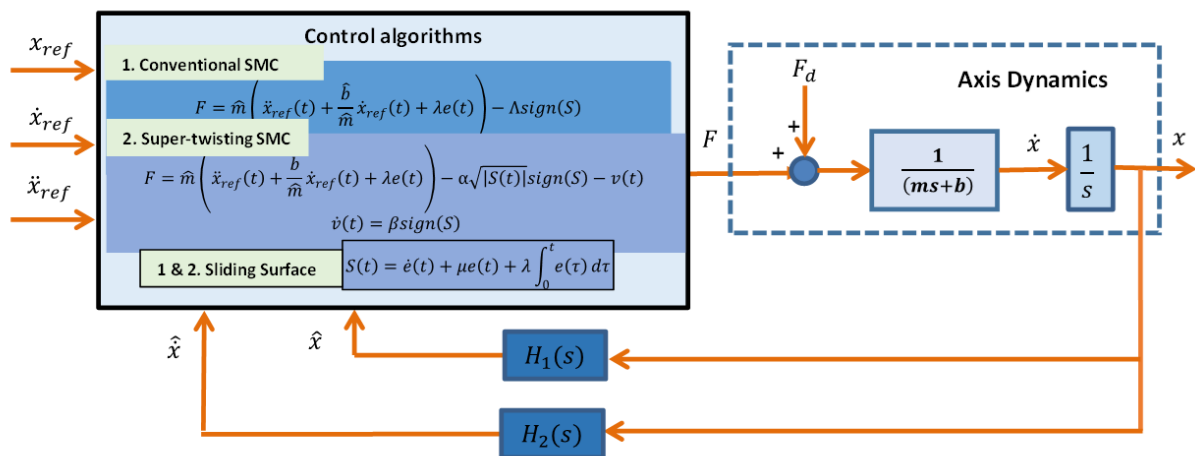


Figure 2. Closed-loop description including feed drive machine tool and SMC algorithms

are provided from CAD/CAM systems or pre-programmed by the engineer. These trajectories may be designed in order to fulfil specifications and, to get smoothness. In order to test the proposed control algorithm sufficient excited signals in the form of sinusoidal waves are chosen as position reference signals, which are widely used in machining. Their first and second derivatives are considered as velocity and acceleration reference signals.

The control algorithm takes the reference signals with certain initial conditions for the position, velocity and acceleration and processes SMC algorithms in a certain sliding surface to generate the control signal, F . Before acting into the system, the control signal acquires the disturbances forces, F_d , namely cutting forces, which are inherently generated by the cutting process. The system outputs the relative position between the tool and workpiece respect to a predefined coordinate system. The position of the system is measured by an encoder, which gives an estimation of the actual value. Similarly, the velocity of the system is also estimated. Both signals are cleaned by low-pass filter in order to damp the influence of high frequencies. In the following loop, the sliding surface and the control algorithms are processed again, keeping the output within the sliding surface while respecting the predefined tolerance despite the disturbances acting on the system. The loop is repeated at every control time interval.

5. Results

The simulations were implemented in Matlab/Simulink environment using the integrated numerical method for solving the Eq. (1)-(9) in continuous time. Continuous time domain simulations are typical approaches in control systems theory in order to analyse the behaviour of the system.

The simulations consist of reference inputs in form of sinusoidal waves, which are movements along individual axes, sinusoidal disturbance due to cutting parameters according to micro-milling processes, and variation of mass of the workpiece due to a material removal process and damping in the process due to the use of lubricants when machining.

Extensive simulations have been carried out in order to evaluate the proposed control algorithm. In the simulations, a sinusoidal reference input signal of amplitude one millimetre (or 2 mm peak to peak) and 3 rad/second of frequency is used to test the control. Disturbances correspond to cutting forces in 2 teeth and 0.9 mm diameter micro-milling tool at 11 520 rpm, 0.9 mm axial depth of cut and 1.08 mm/min feed rate, which are typical in micro milling processes [21].

The following parameters and assumptions have been taken into consideration in the simulation, actual mass and damping $m = 10$ kg, $b = 250$ kg/s, and amplifier and motor force constant $K_t = 2$ A/V, $K_a = 50$ N/A. The parameters of the plant change slightly with time due to variations in the mass during the cutting process, variations in the damping due to lubricant and due to uncertainties in their values. In the simulations the estimated mass is considered as $\hat{m} = 7$ kg and the estimated damping $\hat{b} = 200$ kg/s.

Individually, the control performance hinges on the selection of parameters of the sliding surface, (μ, λ) , how well the parameters of the transfer function have been estimated, namely mass and damping and, the selection of the constant of sign function on the control Λ , for the SMC and the pairs (α, β) for the super-twisting SMC. In this section, just the variation of the sign function parameter Λ , for the SMC and the pairs (α, β) for the super-twisting SMC, are considered to compare both controllers, the other parameters were adjusted as mentioned before and sliding surface parameters are selected as $(\mu, \lambda) = (2, 1)$. For each simulated scenario, four integrated figures are plotted. The upper left figure plots the reference position in dashed red and the actual position in blue, the second one represents the position error, and the third one outputs velocity error and the fourth one is the control signal.

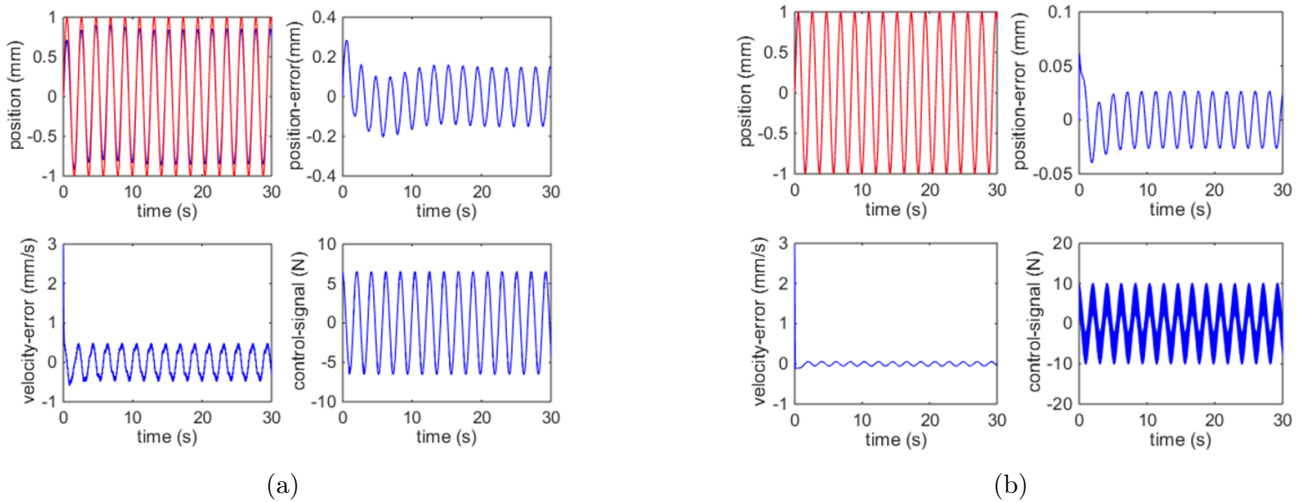


Figure 3. a) Outputs SMC with $\Lambda = 40$, b) Outputs SMC with $\Lambda = 400$

Fig. 3(a) represents the SMC with $\Lambda = 40$ under the influence of the cutting force acting as external disturbance. It can be shown that the control signal is smooth but the tracking error is significant, leading to the system not to follow pre-established tool path references.

In order to deal with error the parameter Λ is increased to 400, as it can be seen in Fig. 3(b). In this case, adequate tracking performance is obtained, however chattering due to high frequencies introduced by the sign function in the control signal appears, as it can be shown in the control signal plot of the Fig. 3(b). The trade-off between precision in tracking the reference signal and chattering limits the control algorithm. To deal with chattering problem, super-twisting SMC has been applied. Fig. 4(a) shows that better performance in tracking the reference signal can be achieved without introducing chattering in the control signal. Balance between tuning control parameters to reach adequate tracking and chattering is required to achieve satisfactory performance indexes. High values of control parameters makes the algorithms more demanding in terms of control power, i.e. amplifiers, and more sensitive to introduce noise to the system.

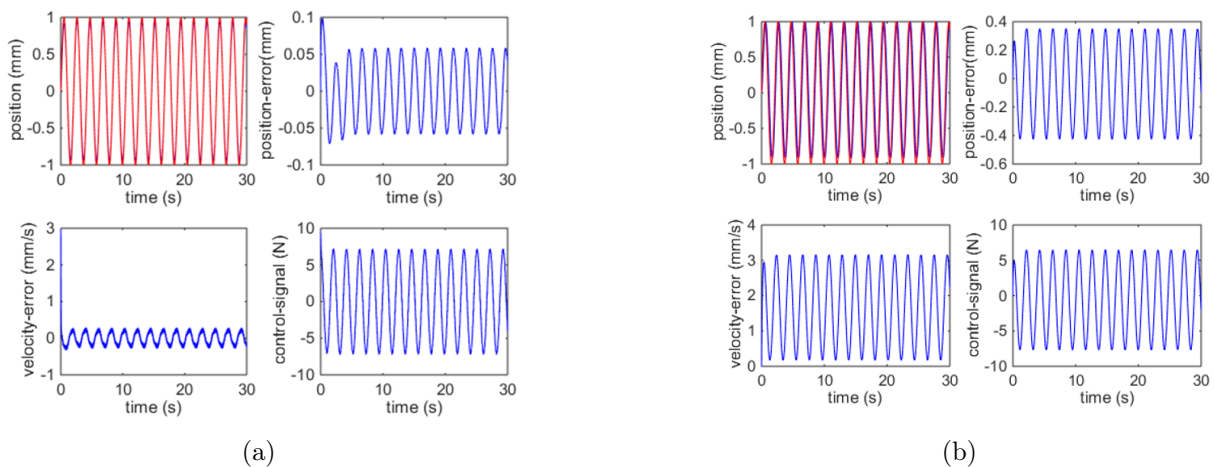


Figure 4. a) Outputs Super-twisting SMC with $(\alpha, \beta) = (200, 200)$, b) Outputs commercial CNC

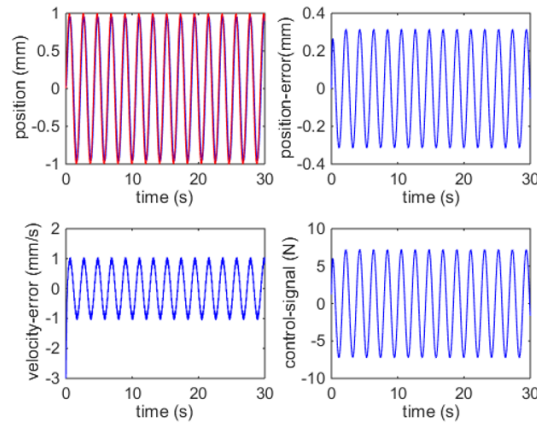


Figure 5. Outputs P-PD cascaded control system

In order to compare the proposed algorithmic methodologies with conventional PID controllers, other two controllers are exposed in this section. The first one is a typical control loop implemented in a state of the art of commercial CNC (Fig. 4(b)), and the second one is the P-PD cascaded control loop [16] (Fig. 5). As figures show, the position or tracking error is considerably appreciated in PID based controllers. In shop floors, these errors are compensated before machining.

6. Discussion and future research paths

Currently, CNCs host PID algorithms to face the tracking control of precision machining. The tendency of precision machining is to achieve each time more accuracy and better tracking performance in machining. The performance of motion of PID control algorithms may be significantly deteriorated by the nonlinear plant uncertainties and unknown external disturbances, compensation of dynamic errors is needed to achieve certain degree of quality [22], so adequate PID-based controllers only achieve limited performance when applied to precision machining. Furthermore, free form trajectories, which introduce high frequency inputs, are required in these processes. The realization of free form trajectories in machining leads to reduced product errors, improving accuracy, and minimize time and costs of the whole process. The programming of these trajectories makes the PID controllers inappropriate for the next generation of machining processes. The SMC algorithms have been exhibited promising performance to deal with these systems and they enhanced previous results.

The PID-type sliding surface controls the bandwidth and setting time of the system, however, increasing the bandwidth of the system will lead to the system to be exposed to noise and acquire vibration frequencies due to external perturbations. A trade-off between bandwidth and rejection of noise and filter frequencies which excites machine tool structure are required. The super-twisting algorithm allows keeping the bandwidth of the system to a maximum value while rejecting noise and disturbance frequencies, which excites the machine tool structure, but it is not influenced by chattering in the control signal compared to classical SMC.

As a result, the following future research paths are considered:

1. Discretise the algorithm to be implemented, testing the feasibility of the provided solution in a test based environment.
2. Propose alternative switching control algorithms, which suits with the problem of machining in order to reject disturbances and follow inputs with high frequency sinusoidal components.
3. Provide intelligent skills to accommodate requirements of the process.

7. Conclusions

In this paper, the super-twisting sliding mode control algorithm with PID-type sliding surface is proposed to deal with the motion tracking of linear motors actuated in micro-milling processes. The micro-milling cutting acts as disturbances into the linear motor, which is composed by mass and damper against inertia of the system. The following key findings can be pointed out:

- Sinusoidal motion tracking simulations demonstrate that the proposed super-twisting SMC controller may improve the performance tracking compared with SMC.
- The PID-type sliding surface balances the bandwidth of the system and settling time response while rejects noise and vibratory frequencies into the system.
- The proposed controller is able to achieve sub-micron accuracy single axis motion tracking depending upon the resolution positioning sensor. The higher resolution the sensor has, the better positioning may be achieved.

8. Acknowledgement

The research was carried out in the frame of the project “EFOP-3.6.1-16-2016-00018 – Improving the role of research + development + innovation in the higher education through institutional developments assisting intelligent specialization in Sopron and Szombathely”. A. Ibeas is grateful to the Basque Government for its support through grant IT1207-19.

9. References

- [1] Y. Altintas, *Manufacturing Automation: Metal Cutting Mechanics, Machine Tool Vibrations, and CNC design 2nd Ed.*, Cambridge University Press, 2012, pp. 250-312. [CrossRef](#)
- [2] C-H. Yeung, Y. Altintas, K. Erkorkmaz, *Virtual CNC system. Part I: System Architecture*, International Journal of Machine Tools and Manufacture 46(10), 2006, pp. 1107-1123. [CrossRef](#)
- [3] S. Gordon, M.T. Hillery, *Development of a high-speed CNC cutting machine using linear motors*, Journal of Materials Processing Technology 166(3), 2005, pp. 321-329. [CrossRef](#)
- [4] M.S. Heydarzadeh, S.M. Rezaei, N.A. Mardi, A. Kamali E, *Motion control of a two-axis linear motor-driven stage in the micro-milling process*, Proc. Inst. Mech. Eng. Part E 232(1), 2016. pp. 65-76. [CrossRef](#)
- [5] V.I. Utkin, *Sliding modes in control and optimization*, Springer-Verlag, Berlin, 1992, [CrossRef](#)
- [6] V.I. Utkin, *Sliding mode control design principles and application to electric devices*, IEEE Transactions Industrial Electronics 40(1), 1993, pp. 23-36. [CrossRef](#)
- [7] J. Rivera, L. Garcia, C. Mora, J.J. Raygoza, S. Ortega, *Super-Twisting Sliding Mode in Motion Control Systems*, In: Andrzej Bartoszewicz, *Sliding Mode Control*, IntechOpen, 2011, Chapter 13, pp. 237-254. [CrossRef](#)
- [8] A. Levant, *Quasi-continuous high-order sliding-mode controllers*, IEEE Transactions on Automatic Control 50(11), 2005, pp. 1812–1816. [CrossRef](#)
- [9] Y. Eun, J. Kim, K. Kim, D. Cho, *Discrete-time variable structure controller with a decoupled disturbance and its application to a CNC servomechanism*, IEEE Transactions on Control Systems Technology 7(4), 1999, pp. 414-423. [CrossRef](#)

- [10] Y. Altintas, K. Erkorkmaz, W-H. Zhu, *Sliding mode controller for high-speed feed drives*, Annals of the CIRP 49(1), 2000, pp. 265-270. [CrossRef](#)
- [11] Y. Altintas, C.E. Okwudire, *Dynamic stiffness enhancement of direct-driven machine tools using sliding mode with disturbance recovery*, Annals of the CIRP 58(1), 2009, pp. 335-338. [CrossRef](#)
- [12] X-C. Xi, W-S. Zhao, A-N. Poo, *Improving CNC countering accuracy by robust digital integral sliding mode control*, International Journal of Machine Tools and Manufacture 88, 2015, pp. 51-61. [CrossRef](#)
- [13] X-C. Xi, G-S. Hong, A-N. Poo, *Improving CNC contouring accuracy by integral sliding mode control*, Mechatronics 20(4), 2010, pp. 442-452. [CrossRef](#)
- [14] C. Choi, T-C. Tsao, *Control of linear motors for machine tool feed drives: experimental investigation of optimal feed-forward tracking control*, Journal of dynamic systems, measurement and control 120(1), 1998, pp. 137-142. [CrossRef](#)
- [15] C. Choi, T-C. Tsao, *Control of linear motor machine tool feed drives for end-milling: Robust MIMO approach*, Mechatronics 15(10), 2005, pp. 1207-1224. [CrossRef](#)
- [16] L. Rubio, A. Ibeas, X. Luo, *P-PI and super twisting sliding mode control schemes comparison for high-precision CNC machining*, 24th Iranian Conference on Electrical Engineering (ICEE), Shiraz, 2016, pp. 1825-1830. [CrossRef](#)
- [17] D. Papageorgiou, M. Blanke, H.H. Niemann, J.H. Richter, *Adaptive and sliding mode friction resilient machine tool positioning – Cascaded control revisited*, Mechanical Systems and Signal Processing 132(1), 2019, pp. 35-54. [CrossRef](#)
- [18] F.J. Villegas, R.L. Hecker, M.E. Pena, D.A. Vicente, G.M. Flores, *Modelling of a linear motor feed drive including pre-rolling friction and aperiodic cogging and ripple*, The International Journal of Advanced Manufacturing Technology 73, 2014, pp. 267-277. [CrossRef](#)
- [19] P.J. Torvik, *On estimating system damping from frequency response bandwidths*, Journal of Sound and Vibration 330(25), 2011, pp. 6088-6097. [CrossRef](#)
- [20] X. Yu, M. Önder, *Recent advances in sliding modes: from control to intelligent mechatronics*, Studies in systems, decision and control, Springer, 2015.
- [21] B. Wu, *Analysis and simulation of micro-milling processes*, Master Engineering Thesis, University of South Wales, Faculty of Engineering, 2013.
- [22] C. Liu, S. Xiang, C. Lu, C. Wu, Z. Du, J. Yang, *Dynamic and static error identification and separation method for three-axis CNC machine tools based on feature workpiece cutting*, The International Journal of Advanced Manufacturing Technology 107, 2020, pp. 2227-2238. [CrossRef](#)

PRODUCT CONFIGURATION SYSTEM DEVELOPMENT FOR CAD/CAM SOFTWARE

László Karker^a, Mátyás Andó^{b*}, Jegan Mohan Sudhan Raj^b

^a ELTE, Faculty of Informatics, Savaria Institute of Technology, Mechanical Engineering BSc, IV. year

^b ELTE, Faculty of Informatics, Savaria Institute of Technology, associate professor

ABSTRACT

The radical development of the industry leads manufacturers to adopt more effective methods to exclude the deficit in their process. The application designed in this research establishes a connection between Autodesk Inventor and Edgecam (Hexagon). In case of the component-group the automatic toolpath generation is efficiently usable even in changing product palette. The perfect CAD model with the suitable toolpath is generated in just 92 seconds. The application takes into account the used technological considerations through the manufacturing. For example, the tool dependent diameter before threading, asymmetric tolerance, chamfer and inner fillet. The program is reliably usable from the first machining because the automatically filled parameters minimizes the possibility of errors. The solution increases the reliability of the quotation (even for ERP systems) because it ensures valid process time and toolset.

Keywords: *CAM, CAD, Engineer intelligence, Group technology, Optimization*

1. Introduction

The pretension of the customers changed in the past 10 years over the variability of the products. In this competitive field of manufacturing, it is needed to adapt to the various challenges and provide multiple ranges of product [1]. The high volume low mix (HVLM) production method, which has large volume of products with lower selection is gradually decreasing in recent years [2]. Due to this trend, the manufactures are tend to adopt new business structures, which will enhance their process effectively and economically.

Even still some of the manufactures are following HVLM method. Hence, the 2nd generation mass-production methods were used to minimize the defect in the process. However, in the 3rd generation mass production method (HMLV- high mix low volume), the six sigma and lean manufacturing techniques are not so effective [3].

In the automation of mass production process, due to the longer manufacturing time, specific targeted solutions are to be generated. They had time to experience and even optimize production through the years, so the waste become minimal. However, as a result of the changed conditions, there will be no more opportunities to utilize this strategy. According to automatization and optimization, the process can be divided into 2 parts: the cutting process and the preparing process. In case of a small series batch production, the preparing process is more important than the production process. For example, in a six-piece series, the preparing process starting from the receipt of technical drawing to the beginning of the cutting process consumes much time compared to the machining time [4].

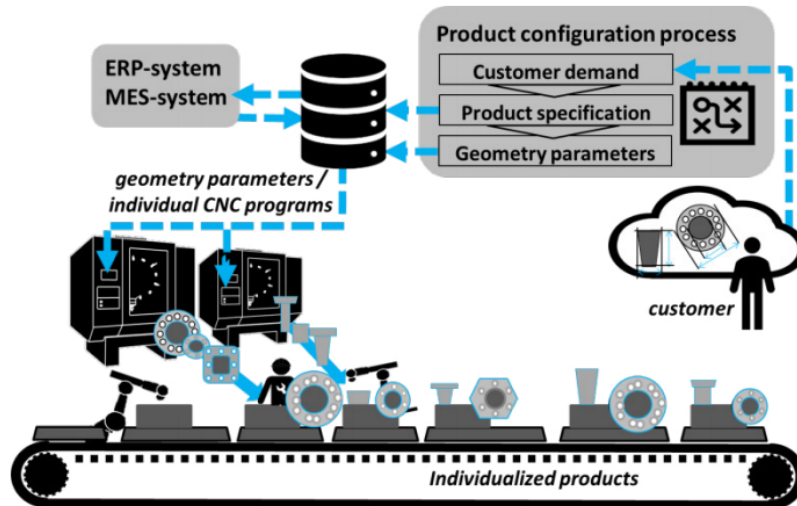


Figure 1. Modern manufacturing system industry 4.0 construction [7]

Following the trends of production, a group technology-based manufacturing concept to start to spread over the past few years [5]. The group technology has a great past and it constantly develops [2, 6]. The grouping of the parts leads to more efficient manufacturing in case of variable and low range productions (HMLV) [3]. Fig. 1 shows a modern structures, which uses a flexible manufacturing system with group-technology, also uses Industry 4.0 elements for their cutting systems [7].

The CNC program is generated step by step, in case of group-technology. Most of the manufacturers generates a so-called G-code manually and the others create individual programs for every product using the CAM system [7]. The modern CAD/CAM systems enhances the effectiveness of these processes while neglecting the repetitive tasks [8]. Recently, every CAD system has some kind of CAM surface, however, the CAD developers may not offer the optimal CAM system for a specific production [9].

In the case of modern automatized systems, the product configuration systems are not commonly used. However, it is proved that using this system, the time required for starting the manufacturing process is drastically reduced [7]. The product configuration system on its graphical surface ensures the quick and efficient modification of the product range. By utilizing these tools, the CAD model and the manufacturing program can be modified for every individual orders. Integrating the data provided by other suppliers (e.g. cutting tool supplier) into a flexible manufacturing systems process is a hard task, even though the CAD and CAM software were developed by the same IT company. When CAD and CAM software developed from different company, the data integration becomes more challenging.

The product configuration system developed in this research is intended to offer a possible solution to these problems. By utilizing this the time required to initiate the machining process can be minimized. It can fix the errors of the unsuitable CAD models and correct the errors from the simplified technical drawings.

2. Material and method

Autodesk Inventor Professional 2018 is used to generate the geometrical model, the same procedure can also be done in the 2020 version. Due to its drawing functions and customizable modeling the 2018 version is preferred in this research. In the case of CAM system, the Edgecam 2020 Software was used due to its inherent flexibility in transferring information between the CAM system and its

strategic module. The graphic programming platform is versatile and the modifications are easier. The CAM system also offers an adaptive tool database, which generates the cutting parameters based on the machining environment.

The programming was generated using C# coding on WPF (Windows Presentation Foundation) using Microsoft Visual Studio. The WPF uses the XAML as surface (frontend) programming language and the C# as a background (backend) programming language [10]. The created program also generates JavaScript-based program, which is accessible by the CAM system and it processes the data of the thread calculator into the cycle.

3. Creating a correct CAD model

Creating a CAD model is an important step to initiate the manufacturing process. The initial step in developing individual and low range products starts from the quotation. The ERP system generates an accurate quote, when the customers' demands such one, as shown in Fig. 1. The cost factor can also be calculated and integrated into the CAD system, based on the parameters of the product and machine. In constructing some of the complex shapes, there are often asymmetrical tolerances, fits, threads, undefined edge on the parts. This should be considered in the CAD modelling phase, otherwise it will lead to a defective part production. If the CAD model is not precise, it may lead to miscalculation in the quotation, which causes financial loss.

It is a common practice to use the ISO 2768 standard in manufacturing, which provides tolerances for linear and angular dimensions without individual tolerance indications. The chosen group sign influences the size of the tolerance. Because the tolerances are symmetric, as for the modelling it does not cause any change. Some of the asymmetric tolerances and fits (ISO 286) information are missing in the model. Hence, the CAD systems generate the model for the basic nominal dimensions. This results to defective part or the settings are to be updated each time for the current interfaces, which requires huge investment in manpower and time.

The improper tooling leads to waste production. Hence, before initiating the production, the tolerances of the tools used for production must be altered with those specified in the drawing. This is one of the most common mistakes in the manufacturing holes. Also, it is an additional problem if there is a thread in the hole, because the core hole and the chamfer are modelled inaccurately. The insert which used to create the inner edges is especially critical. If the radius of the tool nose is larger than specified, then the scrap can arise. According to the ISO 13715 standard, the edge undercut or passing are not included in the CAD model. Hence, the proper selection and modelling of the components is a part of the manufacturing process.

The tool manufactures recommendations are to be considered to develop suitable products, especially in the case of threaded parts. Most of the manufacturers use a full profile insert to generate threaded parts. While creating the model they do not consider the specific cylindrical surface on which the threads are to be generated. This surface are to be generated with a tolerance, so that the diameter of the cylindrical surface will be larger than the nominal size. If this tolerance is not provided in the threaded section the manufactured part may not perform well. It is necessary to define the dimensions within the tolerance limits while programming. The manufacturing program should be created to the middle of the tolerance zone. By following this way, the process can be maintained at a greater accuracy in a long run. This is due to the fact that the actual size alters between the upper and lower tolerance limits, which will reduce the defective parts. The Inventor also provides the ability to specify asymmetric tolerances as well as fits for parametric modelled parts. Also, the model size can be set to generate automatically to the mean of the specified asymmetric fits and tolerances.

4. Basics of the process

In our earlier research [11], a prefabricated material and tool database was created using Edgecam platform. It was tested for the parameter selection in order to confirm the applicability of the database-based technology. Based on these results the development phase is carried out. The operation and structure of the developed product configuration system is shown in Fig. 2.

In Fig. 2, the developed product configuration system is marked in yellow, and the modules which the system is directly connected are marked in orange. The access of the product configuration system is initiated on receiving the order for the product with individual dimensions and thread properties. During the process, the initial step is the calculation of thread in the system. After entering the thread type on the ordered part, the data and tolerances required for machining the thread are displayed in the calculator. The calculator accesses the Inventor database to calculate and retrieve data for that type of thread. Then the shape features of the ordered product are checked and from the menu item corresponding to the part in the configuration system was selected. On selecting from the menu, the parameterized model is displayed in the Inventor, where the changes made are recorded here. From the same menu the parameterized model can be modified to the appropriate size of the product. The thread properties calculated with the calculator are given as inputs in the modification fields. The modification overwrites the model control file attached to the CAD model. It is also used to recheck the accuracy of the dimensions on the part. Once the code is modified, this feature also serves as an effective size control option. A macro can be created in Inventor in order to change the dimensions of the model automatically, which was assigned to the parameterized parts. This macro runs automatically on the logic panel in the Inventor on opening the parts file.

From the model settings, the application generates a JavaScript program. It then fills in the thread machining cycle with data in the CAM system. This adaptively generated program is highlighted in orange in Fig. 2 and is represented as thread parameters. To test the system a parametric component-group was created as shown in Fig. 3. Components of the part-groups are represented in the Fig. 3 as A - step shaft, B - step shaft with groove, C - step shaft with thread, D - step shaft

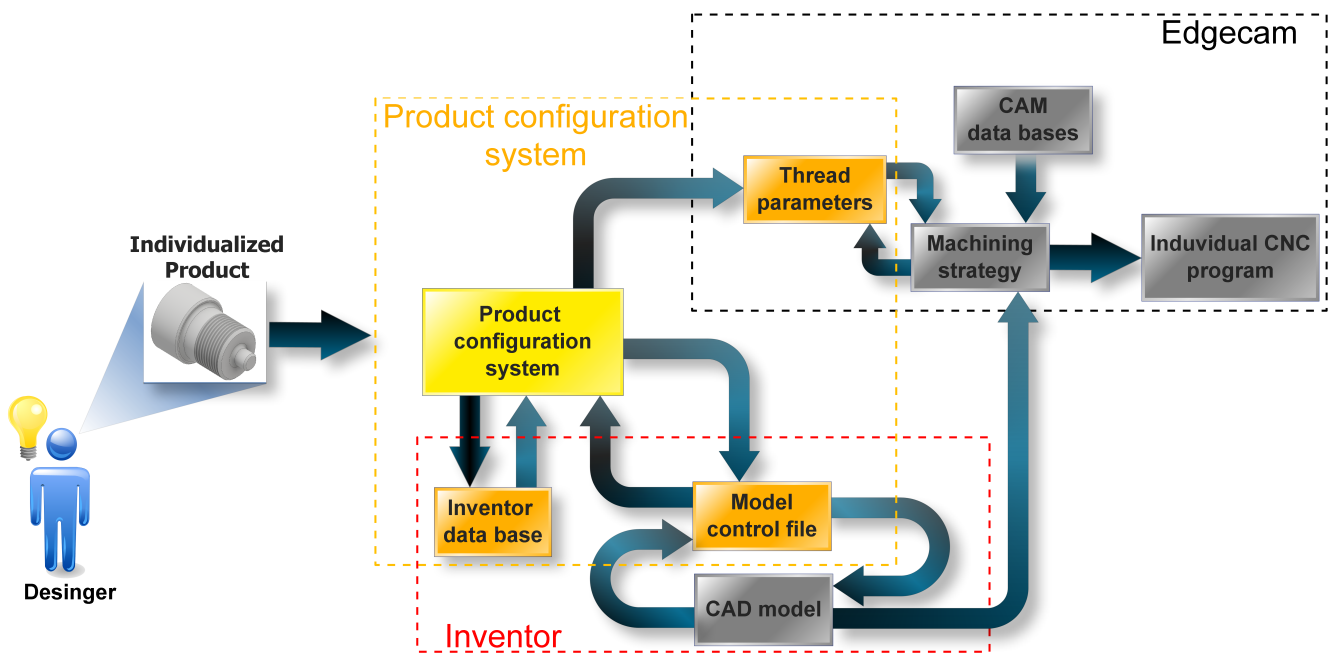


Figure 2. Structure and operation of the product configuration system

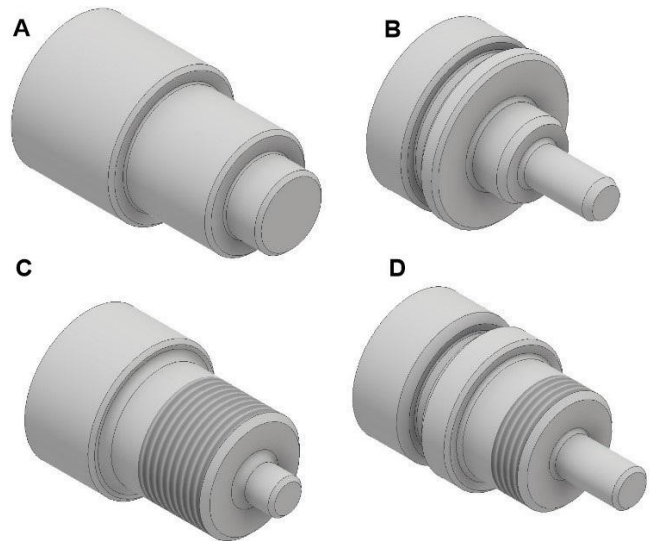


Figure 3. The component-group created for testing

with groove and thread. The dimensions and tolerances of the component can be changed freely. Furthermore, to test the operation a rudimentary machining strategy was developed in Edgecam to check the operation of the process (Fig. 4).

5. Results

From this newly generated product configuration system, the CAD models of the components can be converted into individual product versions according to customer needs. By using the group technology in the application, which allows to manage the manufactured portfolio quickly and efficiently in the graphical interface. The configuration interface is shown in Fig. 5. It also provides the modification of additional geometric features of the model in the graphical interface system. It automatically changes the modeling environment as a result of modification. The accurate CAD model is created automatically. It is clearly seen from the CAD model it is made within the tolerance limits. The design of the system is much more ergonomic and transparent and it provides faster handling compared to the manual modification.

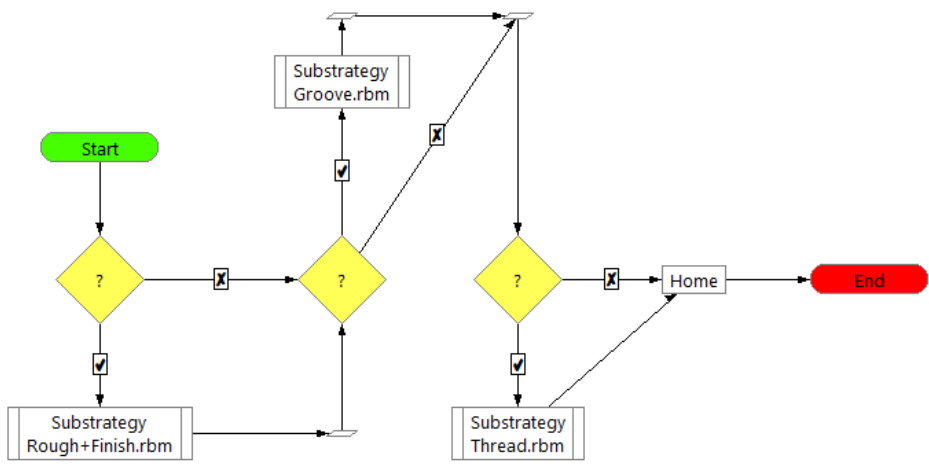


Figure 4. CAM machining strategy used for testing

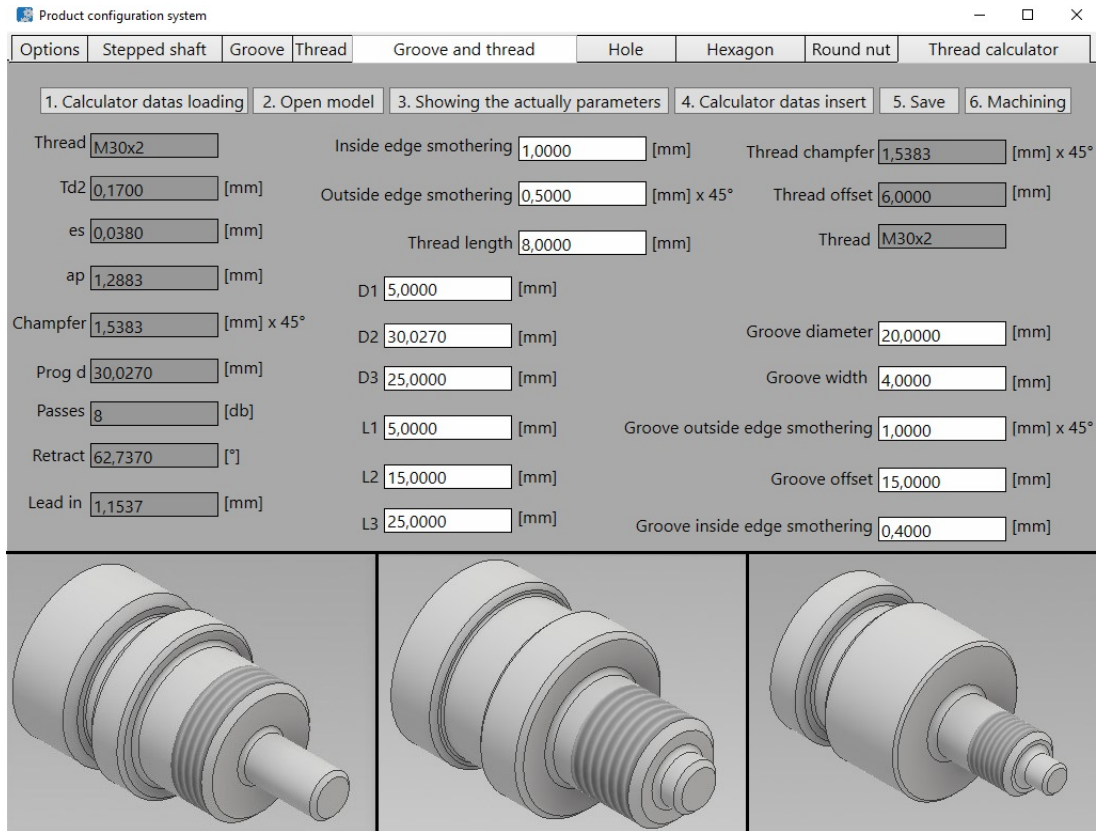


Figure 5. The configuration surface

In the Invertor system the thread diameters can only be assigned based on the thread type from the developer’s data. However, when machining a thread the geometrical dimensions and the thread run out depends on the tool and the machine. The newly developed system addresses this problem. In the testing demonstration that the CAD model and the machining program data calculated with the thread calculator was used. The automatic data transfer greatly increases the speed of production preparation. In addition, we exclude several possible errors that could result from calculations and incorrect settings. The application effectively overcomes the limitations between CAD/CAM systems from different developers and also considers tool manufacturer recommendations. The application has been developed to use a full profile insert. The CAD model is automatically converted accordingly so that the thread on the manufactured product is error free. Fig. 6 shows the CAM paths generated by the system.

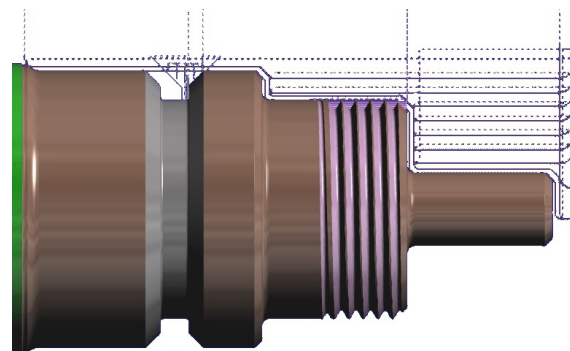


Figure 6. The generated toolpaths

An experienced user can create toolpaths in 90 seconds using this application with pre-opened software. The machining time, that the Edgcam automatically calculated, was 7 minutes 33 seconds. Within this stipulated time, the accurate CAD model is generated. Then the selection of appropriate tools and inserts needed for production happened and the exact machining time was determined. Thus, this software generate quotes reliably for individual product variants with more accuracy in a shorter time.

6. Conclusions

In this paper a newly developed product configuration system was introduced. The time required to prepare for production was drastically reduced to less than 2 minutes. This concept of connecting CAD and CAM systems can be used effectively to serve the current market conditions where the variety of products produced in small quantities. In group-technology-based production, the developed method can be effectively used for programing CNC machines, as the developed program generates accurate CAD model. With the built-in offline thread calculator and export function, the final CNC program can also be created in the CAM software automatically. With this method, quotations can be made based on the exact machining time.

7. Acknowledgement

The project with contract number ED_18-1-2019-0030 (Application-specific high-reliability IT solutions theme area) was implemented with the support of the National Research Development and Innovation Fund, with the support of the Thematic Excellence Program.

8. References

- [1] A. Angelopoulou, K. Mykoniatis, N.R. Boyapati, *Industry 4.0: The use of simulation for human reliability assessment*, Procedia Manufacturing 42, 2020, pp. 296-301. [CrossRef](#)
- [2] I. Ham, E.V. Goncalves, C.P. Han , *An Integrated Approach to Group Technology Part Family Data Base Design Based on Artificial Intelligence Techniques*, CIRP Annals 37(1), 1988, pp. 433-437. [CrossRef](#)
- [3] Patrick de Vos, *Group Technology: Operational Excellence in the Industry 4.0 Era*, Seco Tools AB, Björnbacksvägen 2, 73782 Fagersta Sweden, 2018, [url](#)
- [4] Patrick de Vos, *Steps 6-10 To Peak Performance and Productivity*, Seco Tools AB, Björnbacksvägen 2, 73782 Fagersta Sweden, 2020, [url](#)
- [5] D. Lukic, A. Antic, S. Borojevic, M. Jocanovic, I. Kuric, *Evaluation of the technological effects of application of the FMS elements*, IOP Conference Series: Materials Science and Engineering. IOP Publishing Ltd 749 012018, 2020, [CrossRef](#)
- [6] R.G. Askin, C.R. Standridge, *Modeling and Analysis of Manufacturing Systems*, John Wiley & Sons, 1993, ISBN: 978-0-471-51418-3, pp. 155-156.
- [7] C. Schaede, S. Seifermann, J. Metternich, *Automated generation of CNC programs for manufacturing of individualized products*, Procedia CIRP 72, 2018, pp. 1251-1257. [CrossRef](#)
- [8] T. Dodok, N. Čuboňová, D. Wiecek, *Optimization of machining processes preparation with usage of Strategy Manager*, MATEC Web of Conferences 244(26):02004, 2018, [CrossRef](#)

- [9] T. Dodok, N. Čuboňová, M. Císara, I. Kurica, I. Zajačkoa, *Utilization of strategies to generate and optimize machining sequences in CAD/CAM*, Procedia Engineering 192, 2017, pp. 113-118. [CrossRef](#)
- [10] M. Chand, *What is WPF*, Scharpcorner blog, [url](#)
- [11] L. Karker, M. Andó, *Adatbázis alapú technológiai paraméter választás CAM rendszerekben*, Mérnöki és Informatikai Megoldások|Engineering and IT Solutions I., 2020, pp. 27-33. [Cross-Ref](#)



EÖTVÖS LORÁND UNIVERSITY FACULTY OF INFORMATICS SAVARIA INSTITUTE OF TECHNOLOGY

